SERI/STR-211-2558
(DE85002908)

THIN-FILM POLYCRYSTALLINE SILICON RESEARCH

Final Report for the Period August 1983—August 1984

A Subcontract Report

By
Wayne A. Anderson

October 1984

Work Performed Under Contract No. AC02-83CH10093

State University of New York at Buffalo
Amherst, New York

and

Solar Energy Research Institute
Golden, Colorado

Technical Information Center
Office of Scientific and Technical Information
United States Department of Energy

DISCLAIMER

Available from the National Technical Information Service, U. S. Department of Commerce, Springfield, Virginia 22161.

Price: Printed Copy A04
Microfiche A01

Codes are used for pricing all publications. The code is determined by the number of pages in the publication. Information pertaining to the pricing codes can be found in the current issues of the following publications, which are generally available in most libraries: *Energy Research Abstracts (ERA); Government Reports Announcements* and Index *(GRA* and I); *Scientific and Technical Abstract Reports (STAR);* and publication NTIS-PR-360 available from NTIS at the above address.

Printed in the United States of America
USDOE Office of Scientific and Technical Information
Oak Ridge, Tennessee

SERI/STR-211-2558
(DE85002908)
Distribution Category UC-63

Thin-Film Polycrystalline Silicon Research

Final Report
August 1983 - August 1984

A Subcontract Report

October 1984

Wayne A. Anderson
State University of New York at Buffalo

Prepared under Subcontract No. XL-2-02114-01

SERI Technical Monitor: Y. S. Tsuo

Solar Energy Research Institute
A Division of Midwest Research Institute

1617 Cole Boulevard
Golden, Colorado 80401

Prepared for the
U.S. Department of Energy
Contract No. DE-AC02-83CH10093

TABLE OF CONTENTS

LIST OF TABLES

LIST OF FIGURES

ABSTRACT

This report contains results of research conducted to explore high-efficiency Si solar cell design concepts primarily utilizing high-quality Si substrates, shallow junctions, and passivated surfaces. Computer-aided design was used to select substrate resistivity, implant energy and dose, and A/R coating design. Several possible grid metals were investigated, including magnesium, ytterbium, titanium, and chromium. Ytterbium gave the best results. Several grid designs were used. Textured surfaces were considered to increase short-circuit current density. Ion-implanted cells were furnace-annealed and rapid flash-lamp annealed; best results were obtained from furnace annealing. I-V-T tests revealed conduction mechanisms for excess currents, which led to improved preparation of solar cell edges and increased efficiency. Three designs, MINP, MNP-P, and MINP-P, were examined. The best implanted cell was the MINP design, with 18.5% AA efficiency and 15.6% TA efficiency. The best diffused cell gave 14.9% AA efficiency and 14.0% TA efficiency. Cl-containing I-layers exhibited improved efficiency, increased UV response, reduced surface state density, and better environmental stability.

SUMMARY

Research has been conducted to explore high efficiency Si solar cell design concepts primarily utilizing high quality Si substrates, shallow junctions, and passivated surfaces. Computer aided design was used to select substrate resistivity, implant energy and dose, and A/R coating design. Several possible grid metals were investigated including Mg, Yb, Ti, and Cr. Yb gave the best results. Several grid designs were used, one of which gave 6% shading. Textured surfaces were considered to increase short circuit current density. Ion implanted cells were furnace annealed, and rapid flash-lamp annealed with best results obtained from furnace annealing. Considerable time was spent with I-V-T tests which revealed conduction mechanisms for excess currents. This led to improved preparation of solar cell edges to give increased efficiency.

Three designs, namely MINP, MNP-P, and MINP-P were examined in this work. The best implanted cell was of the MINP design giving 18.5% AA efficiency and 15.6% TA efficiency. The best diffused cell gave 14.9% AA efficiency and 14.0% TA efficiency which is quite good considering the low effort in this work. Cℓ-containing I-layers gave improved efficiency, increased UV response, reduced surface state density, and better environmental stability. These cells exhibited good stability when subjected to high intensity UV and to nuclear radiation. Materials analysis studies of implants and oxides were made using ellipsometry, Auger, and SIMS

facilities located at SUNY-Buffalo, NSF-Bozeman, and SERI. Solar cells were tested for photovoltaic performance at NASA and at SERI. The efficiency values obtained in this work involved cells not having multiple A/R coatings, back surface fields, drift fields, or super high quality substrates.

Application of the MINP design to poly-Si was worked on in the initial stages of research. Efficiency values were about 11% using a truly non-optimum design. Poly-Si is now being implanted with the more ideal design but was not ready at the time of this writing. A Dissertatior by Francis Kai was previously submitted to SERI which fully covers our work on Li and B-passivation of poly-Si. This information is thus not contained herein. Also, work on MIS cells and poly-Si were reported in previous Annual Reports which is not repeated herein.

I - INTRODUCTION

Renewed interest in new ideas for low-cost photovoltaics began in the early 1970's with the NSF RANN Program. Our work on MIS (metal-insulator-semiconductor) junctions began at that time. We were the first to re-examine the M-S structure[1,2] which then led to significant progress by Shewchun, Green, Pulfrey, Fonash, Olsen, and others. Some significant progress in our initial work involved temperature effects,[3] thin metal films,[4] surface studies,[5] thin Si films,[6] application to new types of silicon,[7] conduction mechanisms,[8] and radiation effects.[9] Even though the MIS design reached an efficiency level of 10-13%, the balance of systems cost required efficiency levels in excess of 15% for terrestrial applications.

Our work on the MINP solar cell, in response to a need for higher efficiency, was preceeded by the fine work of M. A. Green who has recently reported an efficiency in excess of 19%. The MINP solar cell utilizes a high quality 0.3 Ω-cm p-type Si substrate, a shallow junction formed by low temperature diffusion or low energy ion implantation, an I-layer composed of thermally grown SiO_2 which may have a uniform thickness of 20 Å or 100 - 200 Å between grid lines, a fine metal grid which may be composed of Ti/Pd/Ag or Yb/Al, and a suitable AR coating. Several different designs have emerged but all serve to give improved UV response and increased V_{oc}.

The MINP cell achieves high efficiency in several ways.

1) The I-layer serves to reduce surface recombination and dark current.

2) The shallow junction gives increased UV response.

3) Careful edge isolation reduces excess currents to increase V_{oc}

4) Further improvement in efficiency are gained through textured surfaces, multiple AR coatings, back surface fields, and drift fields.

The details which follow give information concerning our effort in this area at a very modest funding level. We were thus unable to carry out a thorough study or even begin to optimize the design. In spite of this constraint, an efficiency level near 16% (total area) and 18% (active area) was achieved without use of multiple AR coating, BSF, DF, or other fine tuning techniques.

II - THEORY, DESIGN, AND FABRICATION

This chapter first considers some fundamental theoretical aspects of the MINP solar cell which later lead to a computer-aided design. Solar cell fabrication parameters are then based upon results of computer data.

2-1 Theory and Design

An extensive treatment of solar cell theory is not presented here. A few key equations are discussed to illustrate certain design criteria which have been used. Dark current density may be described by

$$J = J_{01}[e^{V/n_1V_T}-1] + J_{02}[e^{V/n_2V_T}-1] + J_{03}[e^{V/n_3V_T}-1] \qquad (1)$$

where J_{01}, J_{02}, and J_{03} represent diffusion, space charge layer recombination, and another mechanism, respectively. J_{01} may be separated into emitter and base components as given by

$$J_{01} = J_{01b} + J_{01e} \qquad (2)$$

where

$$J_{01b} = \frac{qn_i^2}{N_A} \cdot \frac{D_n}{L_n}\left[\frac{S_n \cosh(X_b) + \frac{D_n}{L_n}\sinh(X_b)}{\frac{D_n}{L_n}\cosh(X_b) + S_n \sinh(X_b)}\right] \qquad (3)$$

and $$J_{01e} = \frac{qn_i^2}{N_D} \cdot \frac{D_p}{L_p}\left[\frac{S_p \,\mathrm{Cosh}(X_e) + \frac{D_p}{L_p}\,\mathrm{Sinh}(X_e)}{\frac{D_p}{L_p}\,\mathrm{Cosh}(X_e) + S_p\,\mathrm{Sinh}(X_e)}\right] \qquad (4)$$

with $X_b = W_b/L_n$, $X_e = W_e/L_p$, S_n & S_p = surface recombination velocities at front and back surfaces, W_b & W_e = thickness of base and emitter regions, and other terms have their usual meaning. For a very thin n-region, $X_e \to 0$, and

$$J_{01e} \simeq \frac{qn_i^2 S_p}{N_D} \qquad (5)$$

provided that $L_p > 1\mu m$. J_{01b} cannot be conveniently simplified unless $W_b < 100\ \mu m$ since $L_n \simeq 500\ \mu m$ for high quality Si. For a typical wafer, $D_n/L_n \simeq 10^3 cm/s << S_n$ with an ohmic contact. Thus,

$$J_{01b} \simeq \frac{qn_i^2}{N_A} \cdot \frac{D_n}{L_n}\,\mathrm{Coth}\left(\frac{W_b}{L_n}\right) \qquad (6)$$

Assuming $W_b/L_n = 1$, $D_n/L_n = 10^3 cm/s$, and $N_A = 10^{17}/cm^3$ we obtain $J_{01b} \simeq 1.2 \times 10^{-12}\ A/cm^2$. J_{01e} may be calculated from (5) using $N_D \simeq 10^{20}/cm^3$ (which is an average value) to give $J_{01e} = 10^{-18}\ S_p$. Thus, a reasonable value of S_p insures that J_{01} is mainly governed by the base region. Proper surface passivation is essential to achieve this result. It must also be kept in mind that S_p is related to surface state density (N_{ss}) by

$$S_p = \sigma\, v_{th} N_{ss} \qquad (7)$$

where σ = capture cross section and v_{th} = carrier thermal velocity. Thus, minimization of N_{ss} is essential to reduce S_p.

J_{02} represents space charge layer recombination given by

$$J_{02} = \frac{qn_i W}{\tau_0} \tag{8}$$

where W = space charge region width and τ_0 = carrier lifetime. We may estimate J_{02} using W = 0.1 μm and τ_0 = 1 μs to obtain $J_{02} \simeq 2 \times 10^{-8}$ A/cm^2. J_{03} represents any additional excess current component. For example, field emission currents at semiconductor edges are known to cause an excess current contribution. Thus, a properly surface passivated solar cell is limited in J_0 by quality of the substrate at high voltage (J_{01b}) whereas lower voltage current values are limited by J_{02}. J_{03} can be eliminated by proper processing of the solar cell.

Short circuit current density (J_{sc}) is given by the familiar equation

$$J_{sc} = q \int_{\lambda_1}^{\lambda_2} \phi(\lambda)\ S.R.(\lambda) d\lambda \tag{9}$$

where S.R. = external spectral response and $\phi(\lambda)$ = solar photon flux distribution. We can then calculate open circuit voltage (V_{oc}) using

$$V_{oc} = n_\ell \frac{kT}{q} \ln\left(\frac{J_{sc}}{J_{o\ell}}\right) \tag{10}$$

where n_ℓ = n-factor under illumination and $J_{o\ell}$ = reverse saturation

current under illumination, both of which are not the same as the dark values. Finally, series (R_s) and shunt (R_{sh}) resistance effects can be included by replacing V by ($V-IR_s$) in equation (1) and adding a term $(V-IR_s) \cdot (A/R_{sh})$ to the right hand side.

Examination of the preceding equations then leads to solar cell design. We wish to decrease S_p and N_{ss} (eqs. 5&7) by proper surface passivation, increase N_D (eq. 5), increase L_n and N_A (eq. 6), increase J_{sc} (eq. 8) by using multiple AR coating or textured surfaces. Other design improvements can be made using BSF, DF, or a thinner substrate.

A computer code was used to design the MINP cell. This code included surface recombination, bandgap narrowing, space charge layer recombination and heavy doping effects. This code was principally used to obtain the doping profile in the base and emitter regions. These profiles are shown in Figures 1 and 2 which recommend a base doping of 7×10^{17} B-atoms/cm^3 and emitter doping of 10^{20} P-atoms/cm^2 for an efficiency of 16% without an AR coating. The computer code also predicts spectral response variation with surface recombination velocity as shown in Figure 3. This clearly illustrates the importance of reducing surface recombination to obtain high spectral response.

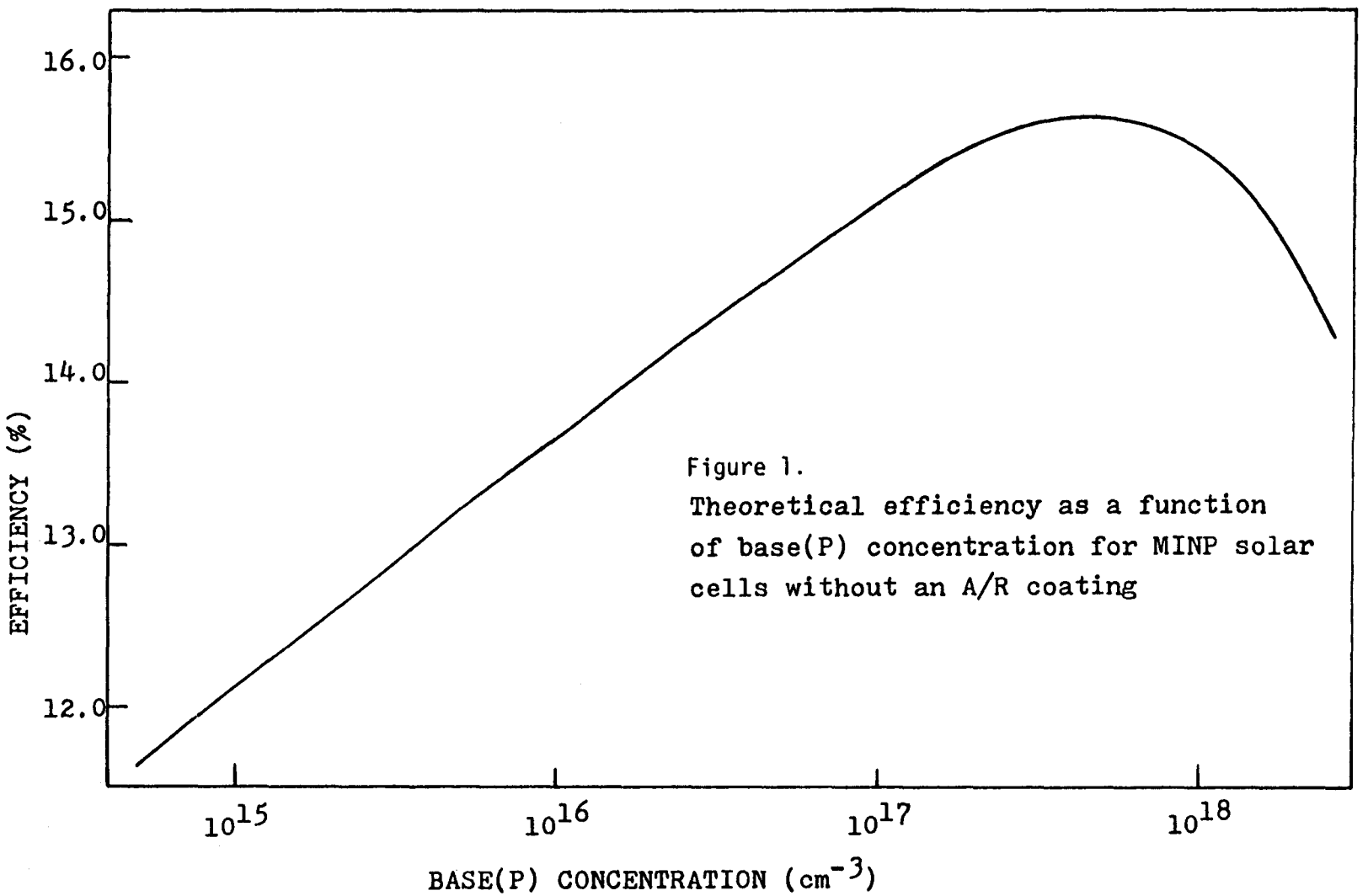

Figure 1.
Theoretical efficiency as a function of base(P) concentration for MINP solar cells without an A/R coating

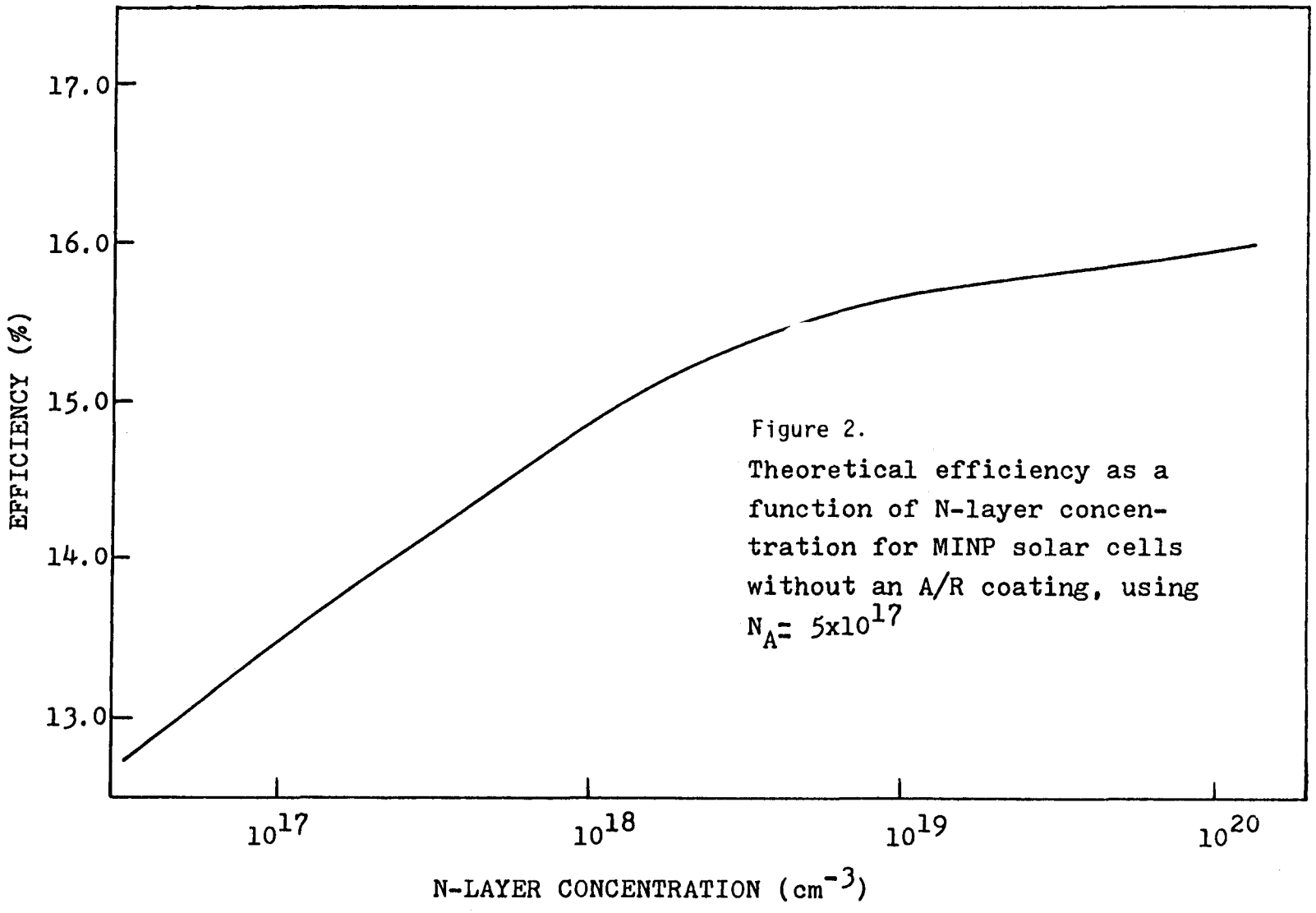

Figure 2.
Theoretical efficiency as a function of N-layer concentration for MINP solar cells without an A/R coating, using $N_A = 5 \times 10^{17}$

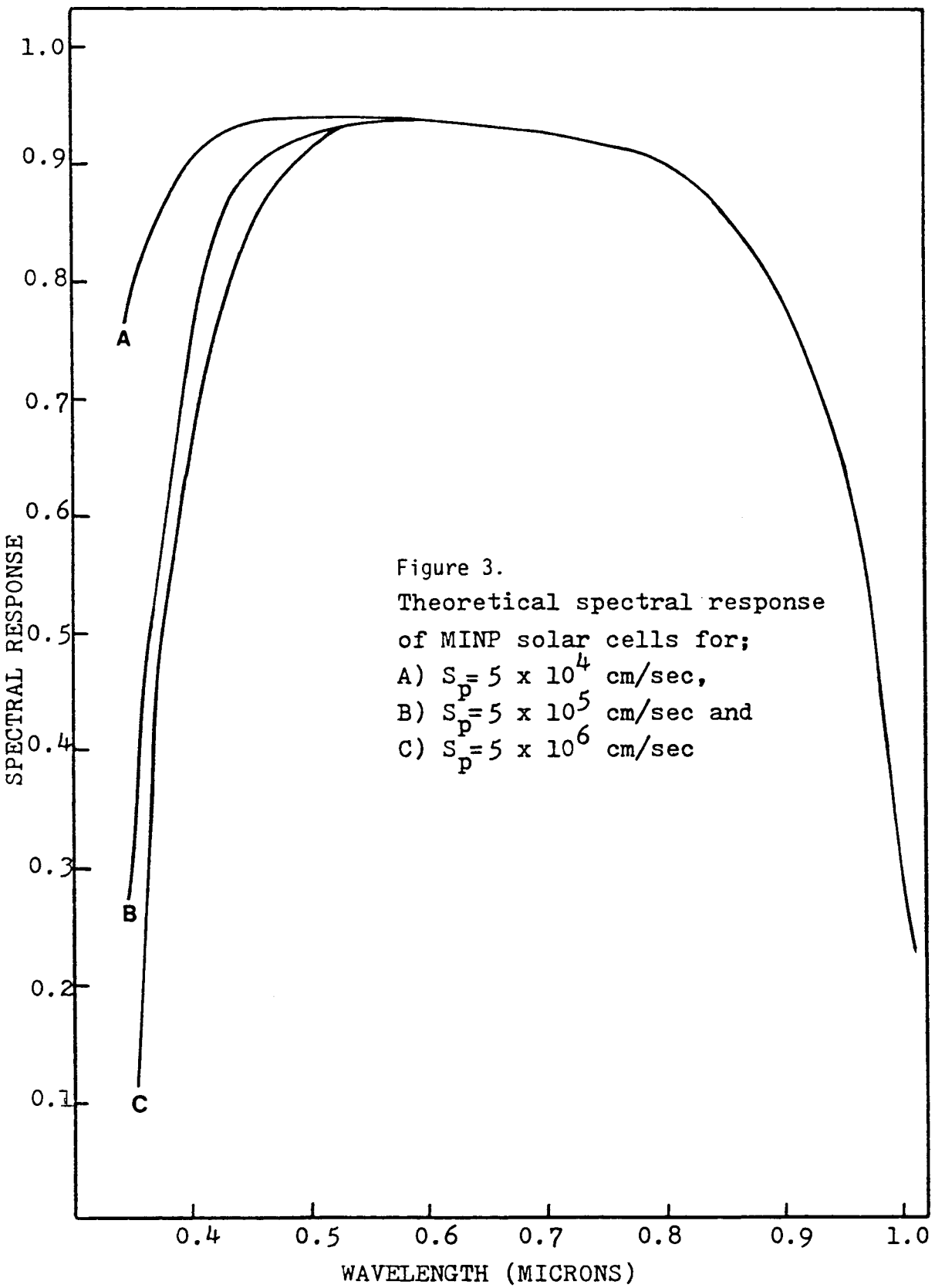

Figure 3.
Theoretical spectral response of MINP solar cells for;
A) $S_p = 5 \times 10^4$ cm/sec,
B) $S_p = 5 \times 10^5$ cm/sec and
C) $S_p = 5 \times 10^6$ cm/sec

2-2 Basic Fabrication Procedure

The quality of the I-layer in MINP solar cells is critical in achieving high efficiency. The surface recombination velocity and U.V. response depend strongly on the passivating oxide layer which control the open circuit voltage[11] and hence the efficiency of the solar cell. The approach used to investigate the role of the passivating oxide layer consisted of fabricating 3 types of cells a) MINP, b) Passivated MNP (or MNP-P) and c) MNP. These designs are shown in Figure 4. The solar cells were fabricated by ion-implanting phosphorous at 5 KeV and 2.5 x $10^{15}/cm^2$ onto 0.3 Ω-cm p-type silicon substrates as suggested by the computer code. The samples were annealed at 850 °C (1/2 hour, N_2 flow) followed by 550 °C (1 hour, N_2 flow) to remove the implantation damage. The back ohmic contact was formed by thermally evaporating Al which was sintered at 500 - 600 °C during which time a thin oxide layer was allowed to grow over the entire n-surface for the fabrication of MINP solar cells. A low work function metal (Yb) followed by Al was used for the grid contact. Thermally evaporated SiO_x served as the antireflection coating for all the cells. The same fabrication procedure was followed for the MNP solar cell except that the oxide was removed after sintering the back contact, prior to the formation of the grid contact. In the case of the MNP-P solar cell, a thick (≃ 300 Å) SiO_2 layer was grown over the entire n-surface. Photolithography techniques were used to remove the oxide in regions where the grid contact is to be formed.

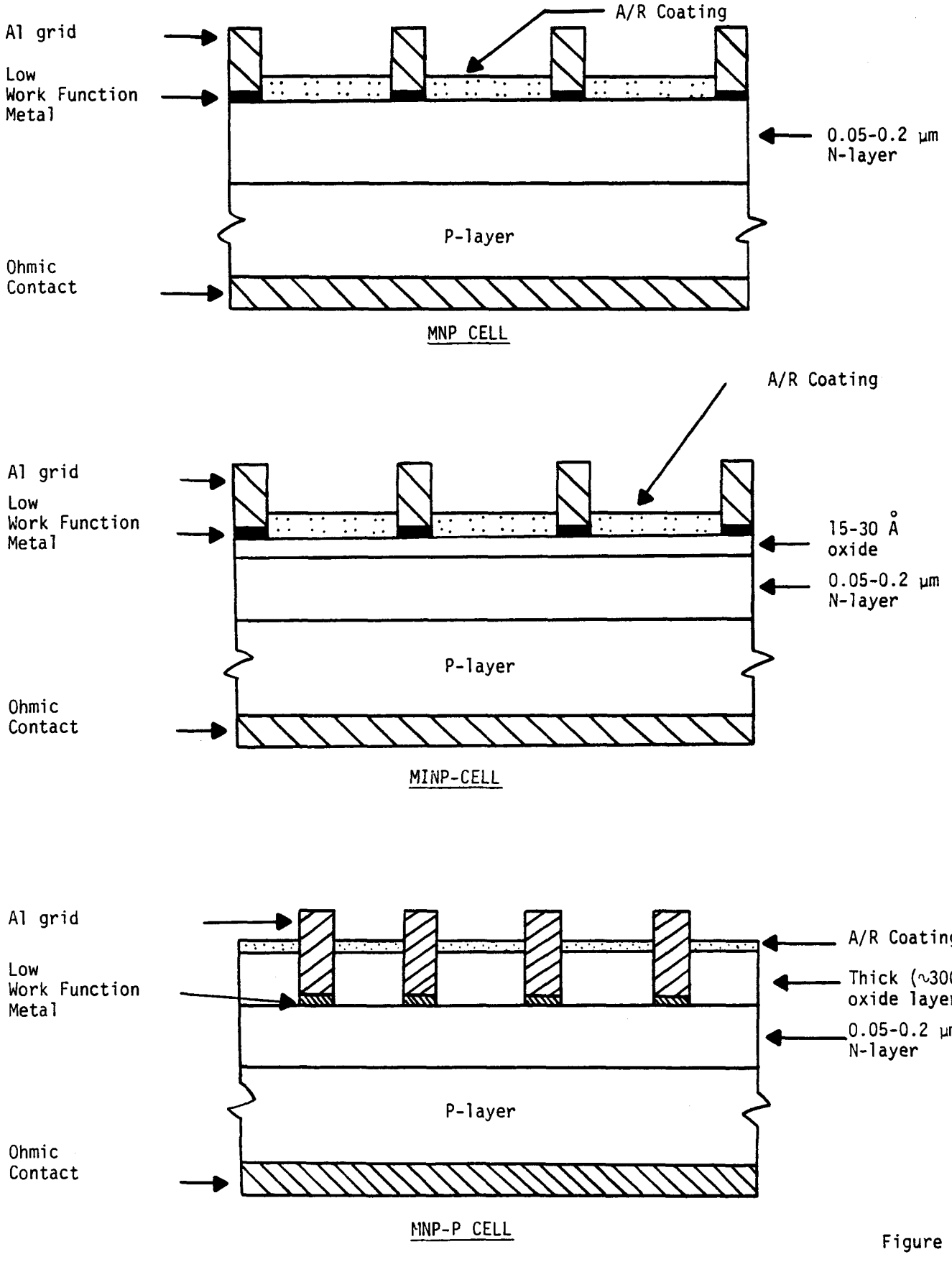
Al grid
Low
Work Function
Metal
A/R Coating
0.05-0.2 μm
N-layer
P-layer
Ohmic
Contact
MNP CELL
A/R Coating
Al grid
Low
Work Function
Metal
15-30 Å
oxide
0.05-0.2 μm
N-layer
P-layer
Ohmic
Contact
MINP-CELL
Al grid
Low
Work Function
Metal
A/R Coating
Thick (~300 Å)
oxide layer
0.05-0.2 μm
N-layer
P-layer
Ohmic
Contact
MNP-P CELL

Figure 4.

The photovoltaic characteristics of a few cells are presented in Table 1. Of these 3 designs, the MINP solar cells show the highest efficiency followed by MNP-P and MNP. As can be seen from Table 1, a passivating oxide layer is required on the n-surface under the grid lines and between grid lines to reduce surface recombination.

TABLE 1

PHOTOVOLTAIC DATA COMPARING 3 CELL DESIGNS

Cell #	V_{oc} (mV)	J_{sc}^{*} (mA/cm^2)	Fill Factor	Efficiency* (%)	Remarks**
703	617	36.9	0.72	16.4	MINP
730	624	35.9	0.73	16.2	MINP
720	610	34.8	0.74	15.8	MNP-P
735	624	34.5	0.74	16.0	MNP-P
729	613	34.3	0.73	15.3	MNP

* AM1 illumination based on active area. Total area is 12% more than active area.

** Implanted using 5 KeV into a 0.3 Ω-cm substrate. Cell edges are scribed.

The fact that the passivating oxide layer results in a better U.V. response can be seen from the spectral response given in Figure 5. This shows the typical MINP cell to be superior to the MNP cell. Also, when the spectral response of the MINP and MNP-P solar cells were compared, it was observed that the MINP cells had a better U.V. response. This suggests that although the MNP-P cells have a thick oxide layer between the grid lines, a thin passivating layer under the grid contact

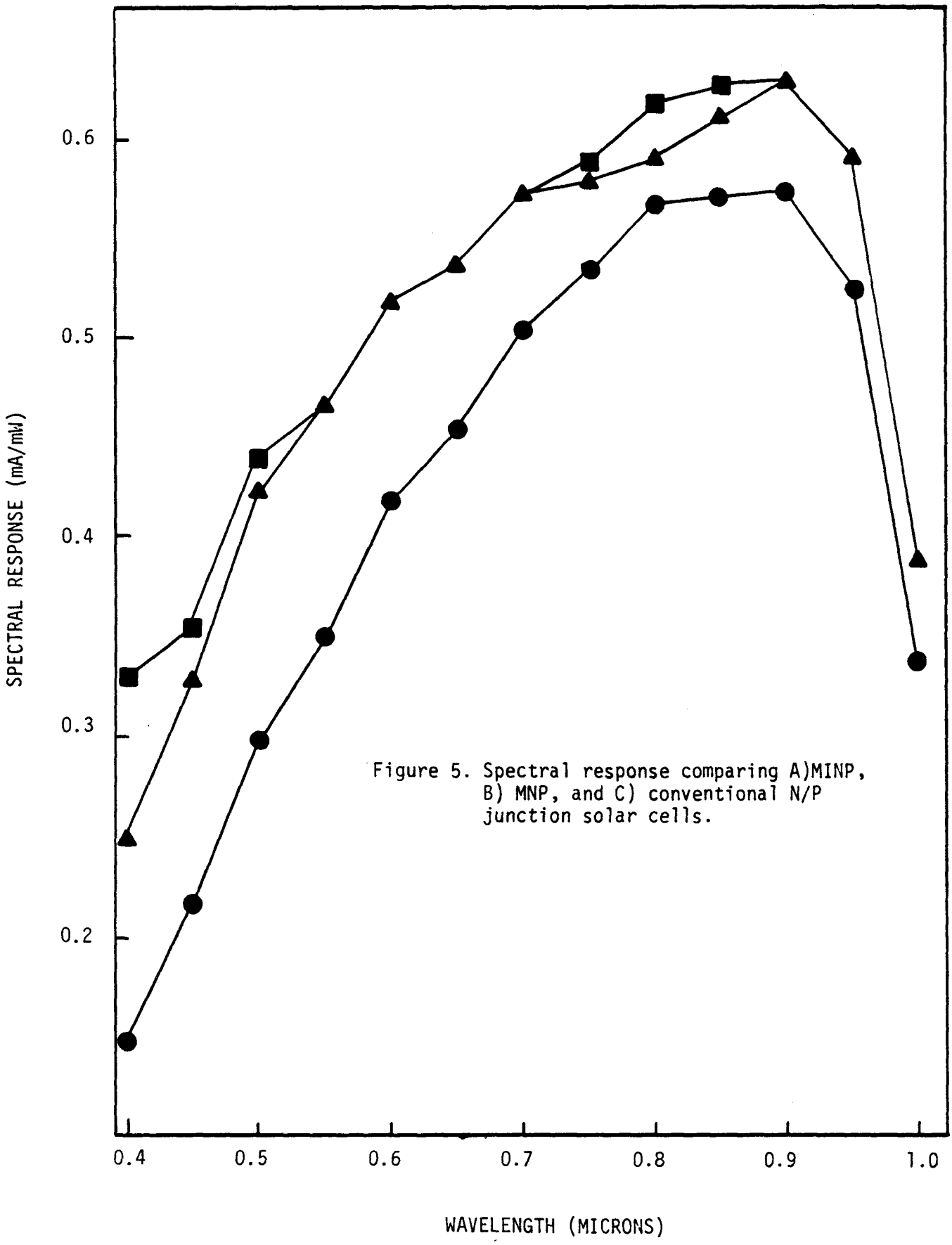

Figure 5. Spectral response comparing A)MINP, B) MNP, and C) conventional N/P junction solar cells.

is essential to minimize surface recombination. This latter design would require first growing a good quality oxide layer ($\simeq$ 200 Å) over the entire n-surface. Using photolithography techniques, the oxide layer where the grid contact is to be formed would be completely removed and a thin ($\simeq$ 15 - 30 Å) SiO_2 layer would be grown in this region. By this method, a thin oxide layer would be present under the grid contact and a thick passivating oxide layer would be present between the grid lines. It is expected that this design would yield better results than the MINP or MNP-P.

III - MODIFIED MINP SOLAR CELL DESIGN

3-1 Ion Implantation

In order to optimize the n-layer concentration and junction depth in fabricating MINP solar cells, 5 different doses and energies were tried for the ion-implantation:

1) As, $2 \times 10^{13}/cm^2$, 25 KeV
2) P, $1 \times 10^{14}/cm^2$, 25 KeV
3) P, $1 \times 10^{15}/cm^2$, 30 KeV
4) P, $2.5 \times 10^{15}/cm^2$, 10 KeV
5) P, $2.5 \times 10^{15}/cm^2$, 5 KeV

Typical results obtained using these different ion-implantation parameters are presented in Table 2. Best results were obtained from the implantation at 5 KeV and $2.5 \times 10^{15}/cm^2$. Higher implant energy causes increased damage in the Si, evidenced by a reduced V_{oc} and FF, and a deeper junction. Implant damage gives increased recombination at high implant energy. A deeper junction also gives reduced U.V. response and a non-optimum doping profile. Even 10 KeV compared to 5 KeV is enough to reduce the quality of the top n-region. An example of the doping profile for a 10 KeV implant is given by the theoretical plot of Figure 6.

TABLE 2

COMPARISON OF DIFFERENT ION IMPLANT CONDITIONS

Cell Number	Ion-Implantation Parameters	Substrate Resistivity (Ω-cm)	V_{oc} (mV)	J_{sc}* (mA/cm^2)	Fill Factor	Efficiency* (%)
496	As, 2 x 10^{13}/cm^2, 25 KeV	(0.8 - 1.2)	560	35.0	0.64	12.5
673	P, 1 x 10^{14}/cm^2, 25 KeV	(1 - 4)	565	29.16	0.68	11.2
694	P, 1 x 10^{15}/cm^2, 30 KeV	(1 - 4)	570	35.6	0.70	14.2
745	P, 2.5 x 10^{15}/cm^2, 10 KeV	0.3	617	31.5	0.74	14.4
738	P, 2.5 x 10^{15}/cm^2, 5 KeV	0.3	629	35.9	0.70	15.9

* Using AM1 illumination and based upon active area. Total area is 12% more than active area. Cell edges are scribed.

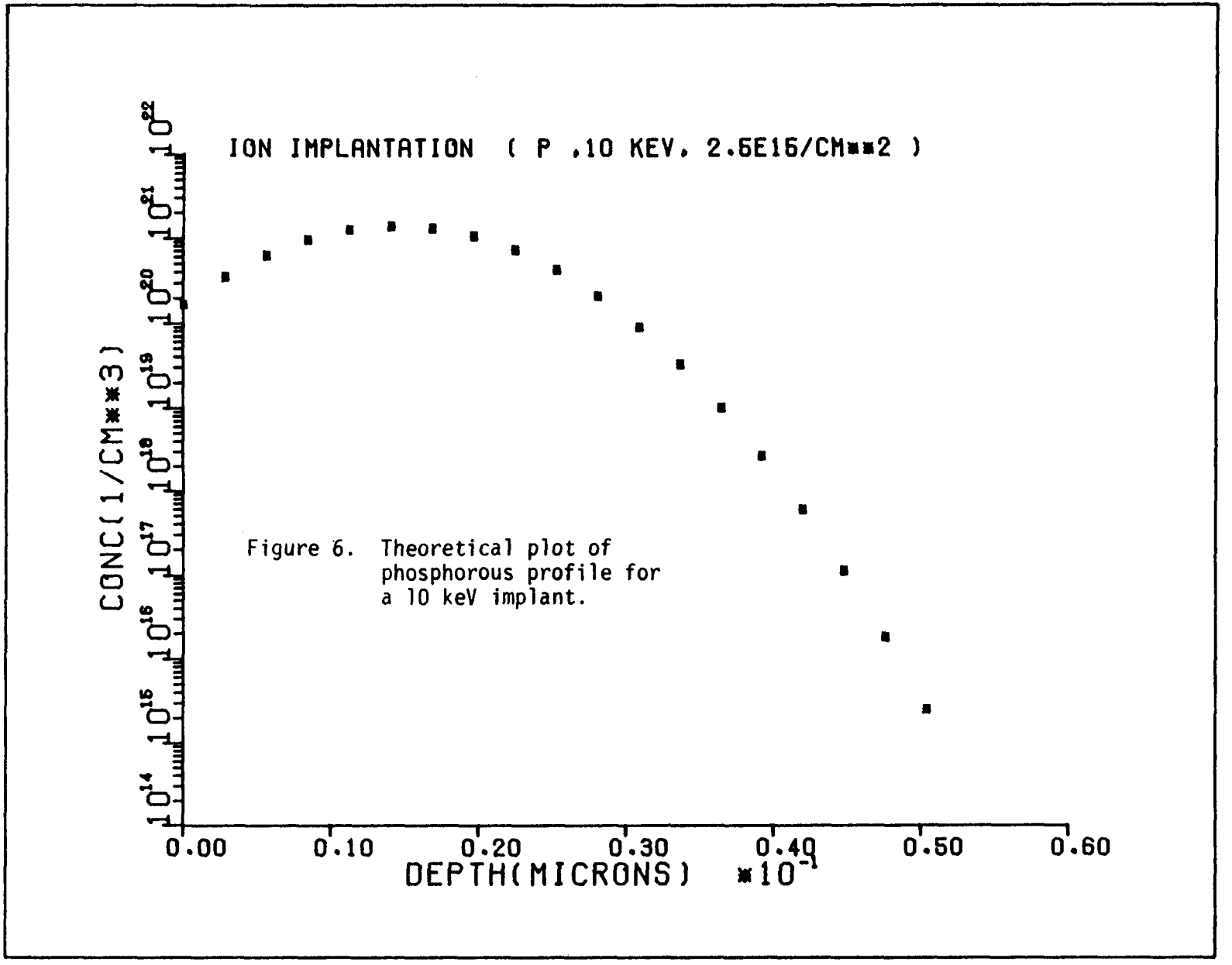

Figure 6. Theoretical plot of phosphorous profile for a 10 keV implant.

3-2 Annealing

The past few years has seen a rapid growth of interest in laser annealing.[12,13] The method involves heating for short times and higher power density that cannot be normally achieved in a standard furnace. Because of the short duration of the heat pulse, the implanted semiconductor may be annealed without appreciable dopant diffusion[14] while still producing a high level of electrical activation. Also, a complete recrystallization of the damage layer can be achieved by laser annealing[14] without reducing the bulk minority carrier lifetime. This section directly compares pulsed laser annealing to furnace annealing in surface passivated, shallow junction, high efficiency solar cells where the surface properties and bulk minority carrier lifetime are critical. The comparison reveals that proper furnace annealing is preferred to the pulsed laser.

MINP solar cells were fabricated on 0.3 Ω-cm float-zone silicon substrates to compare pulsed laser annealing and furnace annealing. Laser annealing was done using a pulsed excimer laser (λ = 308 nm) by scanning the silicon wafer with over-lapping 1/2 x 1/2 cm pulses. Energy density values of 1.04, 0.92 and 0.79 J/cm^2 were evaluated in this study. The furnace annealing was done using either of the following sequences: (a) 850 °C (30 min. in N_2 flow) + 550 °C (1 hr. in N_2 flow); (b) 550 °C (2 hrs. in N_2 flow), 850 °C (15 min. in N_2 + O_2 flow), 550 °C (2 hrs in N_2 flow). The two furnace annealing sequences produced comparable photovoltaic response on identically fabricated cells. In each case, 2 MINP cells, one on a laser annealed substrate and the other on a furnace annealed

substrate, were simultaneously fabricated to compare the effects of the two annealing techniques. Thus, all steps are identical except for the annealing procedure. The results are presented in Table 3. In order to evaluate the degree of the surface recrystallization by laser annealing, reflectance measurements at normal incidence were performed on the three laser annealed substrates using a He-Ne laser. The results of these measurements are presented in Table 4 with additional measurements performed on a furnace annealed substrate (D) and a substrate (E) which received no annealing after the ion implantation.

Table 3 shows that the short circuit current density (J_{sc}) is high for the laser annealed cells. A comparison of this data with the reflectance data of Table 4 shows that cells fabricated on substrates with high reflectance, as in substrate C, gave high short circuit current density. This can be explained by the fact that a high reflectance implies the presence of an amorphous layer, which has a higher absorption of light than does crystalline material, due to an incomplete recrystallization of the damaged layer. In spite of producing high current density, all laser annealed cells exhibited a poor ultraviolet response (Figure 7), as compared to the furnace annealed cells, which could be due to increase of recombination in the surface layer. The improved IR response compensated for the poorer UV response to give increased J_{sc} in laser annealed samples. Excess recombination currents are further evidenced by the poor open circuit voltage (V_{oc}) in cell #768. As seen from Table 4, all laser annealed substrates show a higher re-

TABLE 3

EXPERIMENTAL DATA COMPARING CELLS USING LASER VS. THERMAL ANNEALING

Cell #	Annealing Conditions	V_{oc} (mV)	J_{sc}* (mA/cm^2)	Fill Factor	Efficiency* (%)	J_{od}** (A/cm^2)	n_d	J_{ol}** (A/cm^2)	n_1
757	Laser Anneal (A)	614	32.1	0.73	14.4	1.25×10^{-7}	1.97	5.4×10^{-10}	1.31
758	Furnace Anneal Sequence (a)	615	31.5	0.76	14.8	4.82×10^{-9}	1.59	5.07×10^{-11}	1.17
768	Laser Anneal (C)	596	37.0	0.75	16.5	1.31×10^{-7}	1.95	1.55×10^{-9}	1.35
769	Furnace Anneal Sequence (b)	626	35.1	0.80	17.5	2.63×10^{-10}	1.35	1.37×10^{-11}	1.11
773	Laser Anneal (B)	614	35.7	0.69	15.0	2.14×10^{-7}	2.10	4.67×10^{-8}	1.74
774	Furnace Anneal Sequence (b)	614	35.9	0.70	15.5	2.6×10^{-7}	2.16	3.01×10^{-9}	1.46

* Based on an active area of 1.84 cm^2. Total area is 12% more than active area.

** Using $J = J_o \left[\exp\left(\frac{qV}{nkT}\right) - 1\right]$

TABLE 4

REFLECTANCE FROM Si SURFACE USING A He-Ne LASER

	Laser A	Laser B	Laser C	Furnace Annealed D	No Annealing E
Reflectance (%)	32.0	32.2	34.4	31.1	45.1

Laser A = 1.04 J/cm^2, B = 0.92 J/cm^2, C = 0.79 J/cm^2.

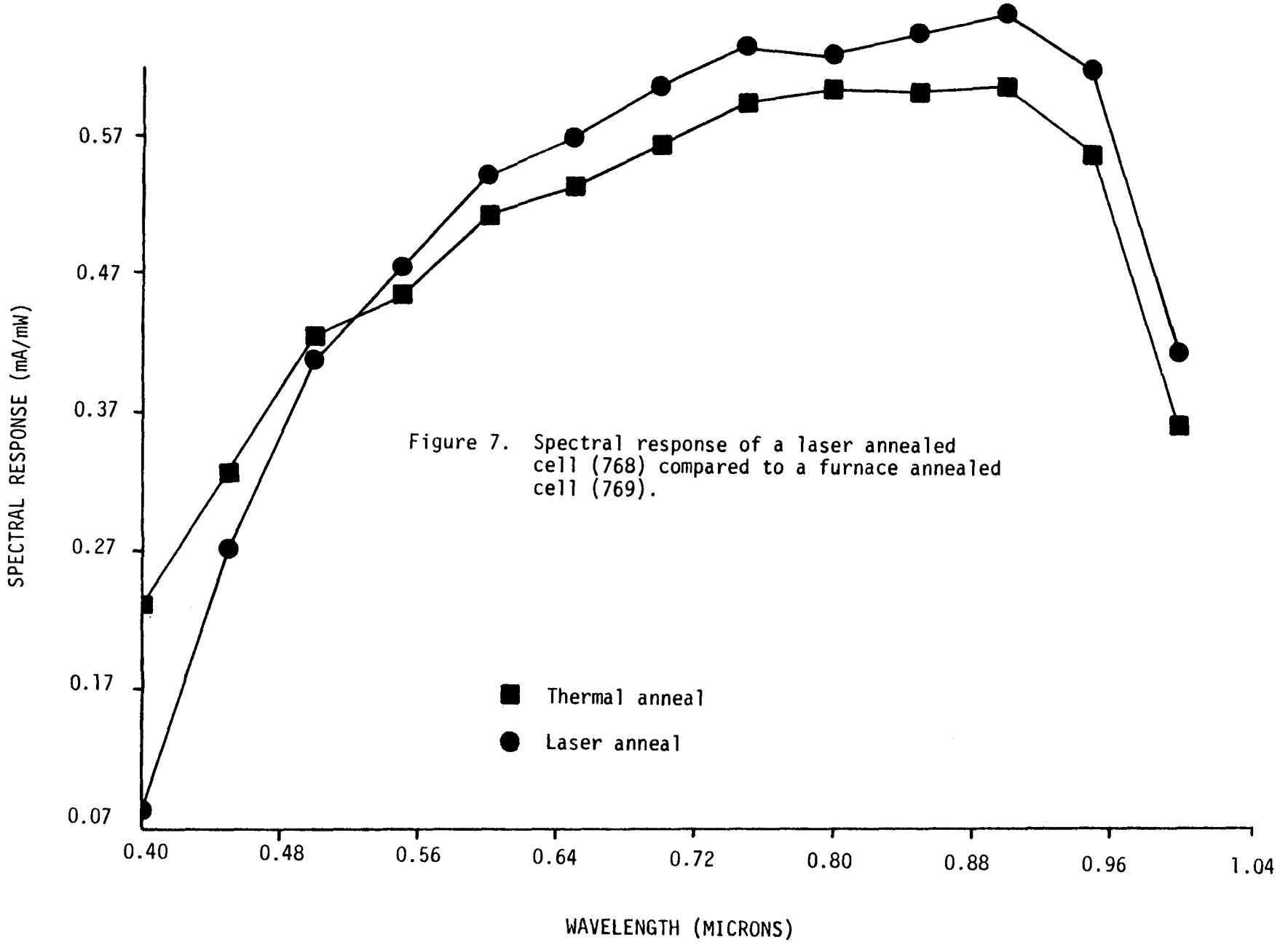

Figure 7. Spectral response of a laser annealed cell (768) compared to a furnace annealed cell (769).

flectance than the furnace annealed sample (D). Thus, furnace annealing appears to achieve a higher degree of recrystallization.

Apart from recrystallization of the amorphous layer, the other critical factor to be achieved by annealing is electrical activation of the dopant atoms. A measure of this factor in a solar cell is the magnitude of ideality factors n_d and n_l in the dark (d) or under illumination (l) and the corresponding saturation current density values J_{od} and J_{ol}. These quantities were obtained for all cells from J-V and J_{sc} - V_{oc} data as presented in Table 3. In most cases, the laser annealed cells showed higher n-factors and J_o values. This could be due to incomplete electrical activation of the dopant atoms, incomplete recrystallization, or a distortion of the designed surface electric field profile. Such high n-factors were previously reported[14] for diodes fabricated on As-implanted laser annealed substrates. Also, a degradation in the electrical activation of the dopant atoms in laser annealed diodes can occur after the 500 - 550 °C step during the solar cell fabrication process similar to that reported elsewhere.[15,16]

Current-voltage-temperature data from 100 °K - 400 °K, in the dark and under illumination, were taken for two MINP cells which were simultaneously fabricated. One of the cells was fabricated on a laser annealed substrate while the other was fabricated on a furnace annealed substrate. Analyses of this data leads[17] to the determination of activation energy ϕ (under dark) and ϕ' (under illumination). The values of ϕ for the laser annealed and furnace annealed cell was 0.52 eV and 0.75 eV, respectively, while ϕ was

1.04 eV and 1.1 eV, respectively. This suggests that the laser annealed cells have a different conduction mechanism in the dark due to the presence of excess recombination centers, but under illumination, when the trapping centers are filled, both cells exhibit identical behavior.

We conclude that solar cells fabricated on furnace annealed substrates show a higher efficiency as compared to those fabricated on companion pulsed laser annealed ones. The high short circuit current density obtained in the laser annealed cells is attributed to a higher infrared response since carrier lifetime is not degraded by high temperature thermal annealing. Unfortunately, laser annealing gives a reduced UV response, reduced V_{oc}, and reduced fill factor due to distortion of the surface electric field profile which hinders carrier collection and increases excess current components such as recombination. This is further evidenced by increased ideality factor, increased reverse saturation current and reduced built-in-potential in laser annealed diodes. Pulsed laser annealing is probably not preferred in high efficiency surface passivated cells where fine tuning of performance is so critical. The higher reflectance in laser annealed substrate C and the higher current in cell #768 are attributed to the existance of an amorphous layer since annealing was incomplete at the lower power level.

A similar study was performed using rapid (flash-lamp) annealing. The annealing was performed by V. B. Rao at Cray Research with a tungsten-halogen lamp having a power of 2KW. Unfortunately, the long wavelength

nature of the lamp resulted in large energy release deep within the wafer which reduced the diffusion length. Reports have been made concerning rapi annealing for solar cells in which short wavelength pulses were used. These results were also not encouraging which may be due to the need of a more careful study. In principal, the technique should be quite good.

3-3 Improved I-Layer Using a TCE - Oxide

The addition of a hologenic species during dry oxidation results in significant improvements in the electronic properties of the oxide and of the underlying silicon. A variety of chlorine-bearing species can be used for this purpose, the most common being chlorine gas and anhydrous hydrogen chloride.[18,19] Lately, there has been considerable interest in trichloroethylene (TCE) since it is less corrosive and can be readily handled in a bubbler arrangement.

In order to evaluate oxides grown in a TCE plus dry O_2 atmosphere, MNP-P solar cells were fabricated simultaneously on two substrates, one passivated using dry O_2 while the other passivated using dry O_2 plus TCE vapors. The latter type of oxide growth was done as follows: Nitrogen was bubbled through TCE in a bubbler and the resulting vapors along with dry O_2 were fed into the furnace tube containing the silicon substrate. The TCE oxidation was performed at 850 °C for 30 - 45 minutes. Once the oxidation was performed using either technique, the cells were fabricated using photolithographic techniques to etch away the oxide in regions where the metal grid is present. The photovoltaic data for cells fabricated on substrates passivated using dry O_2 (MNP-P-0) and those passivated

using dry O_2 plus TCE vapors (MNP-P-T) are presented in Table 5. As can be seen from the table, MNP-P-T cells proved to be superior compared to MNP-P-O type of cells. All of these cells, however, have a low efficiency from the presence of a non-optimum A/R coating due to the presence of a $\simeq$ 100 Å SiO_2 layer on the Si surface prior to depositing the A/R coating. The use of multiple A/R coatings would be helpful here.

More detailed data, shown in Table 6, are given for the two cells in each group having the best dark and light I-V data. There is no significant difference in data for MNP-P-O and MNP-P-T cells when considering J_{od}, $J_{o\ell}$, n_d and n_ℓ values. Most significant changes relate to V_{oc}, J_{sc} and η-values which are better for MNP-P-T compared to MNP-P-O cells. This trend may be due to improved UV spectral response, shown in Figure 8, for the MNP-P-T cells which is related to reduced surface state density discussed in the next paragraph.

In addition, surface state measurements were performed on MOS diodes having a 100 - 120 Å oxide grown in a) TCE plus dry O_2 atmosphere and b) dry O_2 atmosphere. These measurements show that the surface state density is lower (1.4×10^{11} eV^{-1} cm^{-2} at mid-gap) for type a) diodes than type b) diodes (4.0×10^{11} eV^{-1} cm^{-2} at mid-gap) as shown in Figure 9. The exact mechanism for the oxidation in the TCE-O_2 mixture is not well understood but a possible explanation is the conversion of TCE into chlorine by the following reactions:

TABLE 5

SOLAR CELL PHOTOVOLTAIC DATA

Cell Number	V_{oc} (mV)	Fill Factor	I_{sc} (mA)	J_{sc} (mA/cm^2) AA	J_{sc} (mA/cm^2) TA	Efficiency (%) AA	Efficiency (%) TA	Remarks
765	631	0.80	67.5	36.7	30.7	18.5	15.5	MINP-SPIRE after fabrication
765[a]	623[a]	0.80[a]	64.0[a]	34.8	29.1	17.3	14.5	some degradation
795[b]	626[b]	0.76[b]	89.2[b]	41.3	38.8	14.3	13.5	MINP
769	626	0.80	64.5	35.1	29.3	17.5	14.6	MINP
786	622	0.73	79	36.4	34.3	16.5	15.6	MINP
770	586	0.72	67.0	36.4	30.4	15.4	12.9	MINP (Textured Surface) (3 were made having the same results)
756	622	0.78	63.0	34.3	28.6	16.6	13.9	MNP-P-T (TCE Oxide)
735	624	0.74	63.5	34.5	28.8	16.0	13.4	MNP-P-O (Std. Oxide) (see Table for more details)
782	597	0.76	60.0	32.6	27.3	14.9	12.5	MNP-P-O (Std. Oxide)
783	606	0.78	63.5	34.5	28.8	16.4	13.7	MNP-P-T (TCE Oxide)
775	617	0.78	64.5	35.1	29.3	17.0	14.2	MNP-P
776	615	0.77	63.5	34.5	28.8	16.4	13.7	MINP-P
PDS-7	607	0.70	53.4	29.0	24.2	12.5	10.4	Diffused MINP
PDS-9	614	0.74	52.0	28.3	23.7	12.8	10.7	Diffused MINP
PDS-12	618	0.76	72.0	31.9	29.8	14.9	14.0	Diffused MINP

Note: AA = Active area = 1.84 cm^2, TA = Total area = 2.2 cm^2.
Illumination = 100 mW/cm^2 ELH lamp (AM1) except for #795.
#795 and 786 have TA = 2.2 cm^2 and AA = 2.08 cm^2.
PDS-12 had TA = 2.4 cm^2 and AA = 2.3 cm^2.

a) Values confirmed at SERI (AM1)

b) Values confirmed at NASA (AMO)

TABLE 6

COMPARING MINP, MNP-P-T AND MNP-P-O CELLS

Cell #	J_{od} (A/cm^2)	n_d	J_{ol} (A/cm^2)	n_l	Remarks
772	2.4×10^{-10}	1.28	2.02×10^{-11}	1.09	MNP-P-O
782	1.18×10^{-9}	1.42	9.8×10^{-12}	1.05	MNP-P-O
765	2.8×10^{-10}	1.35	4.1×10^{-13}	0.96	MINP-SPIRE
786	5.0×10^{-8}	1.95	5.1×10^{-11}	1.17	MINP
795	4.8×10^{-8}	1.95	4.9×10^{-11}	1.17	MINP
756	7.14×10^{-9}	1.65	5.38×10^{-11}	1.18	MNP-P-T
783	7.91×10^{-10}	1.39	7.96×10^{-12}	1.05	MNP-P-T

AVERAGE STABILITY VALUES

Cell Type	ΔV_{oc} (%)	ΔJ_{sc} (%)	ΔFF (%)	$\Delta\eta$ (%)	Average Number of Days
MINP	1.30	2.3	1.2	4.7	90
MNP-P-O	0.59	1.9	1.0	1.9	130
MNP-P-T	0.16	1.4	1.3	1.4	75

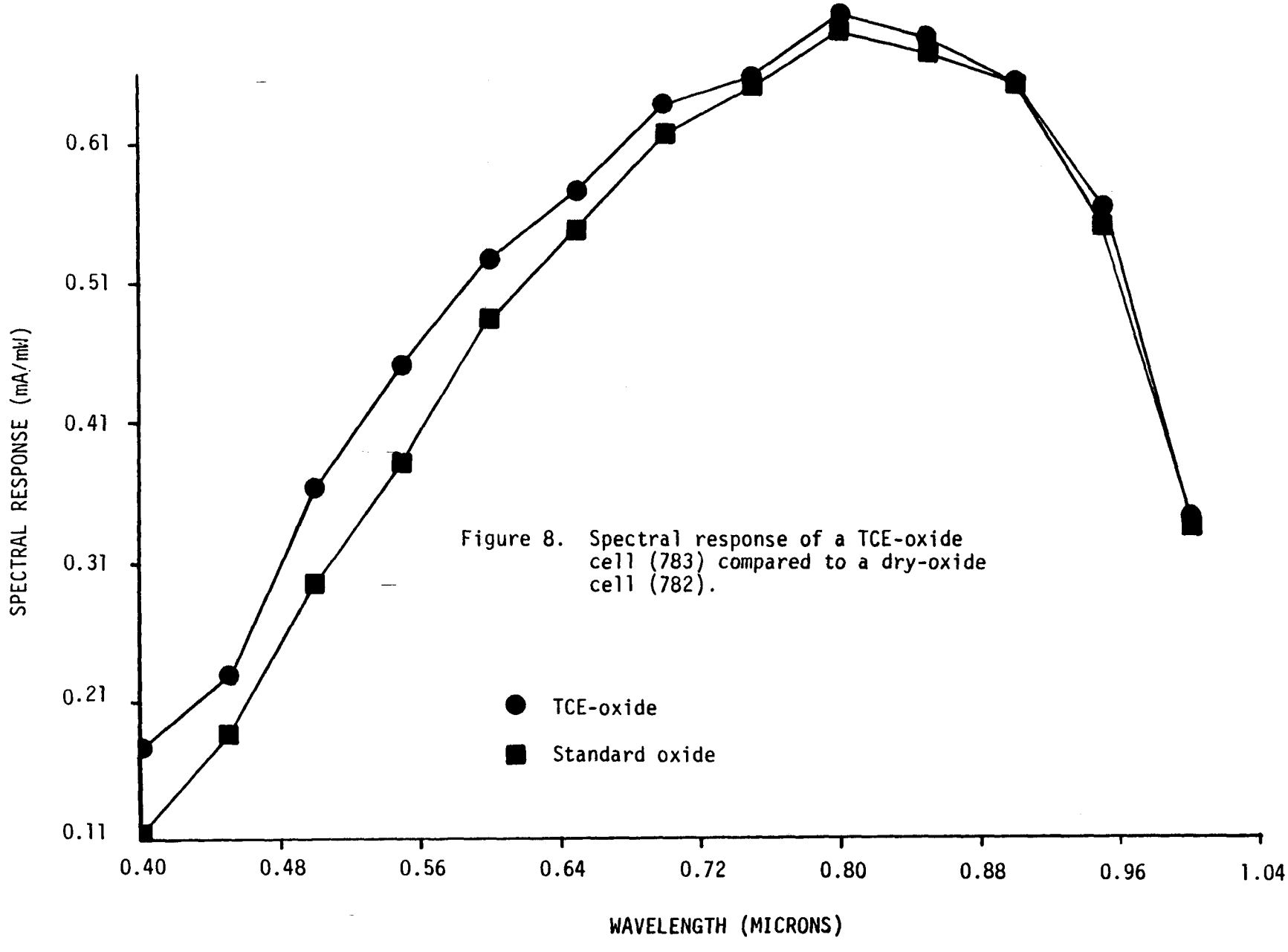

Figure 8. Spectral response of a TCE-oxide cell (783) compared to a dry-oxide cell (782).

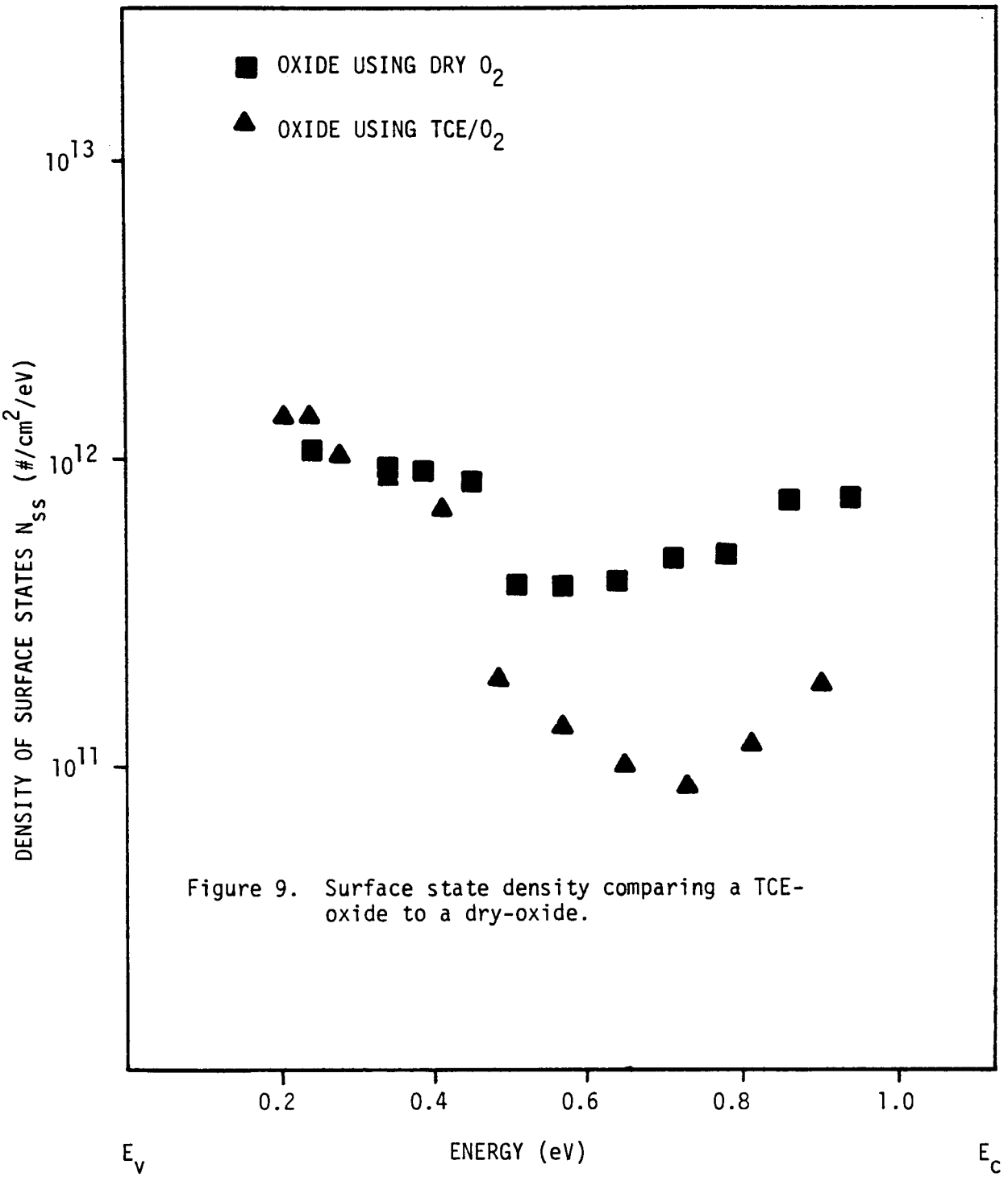

Figure 9. Surface state density comparing a TCE-oxide to a dry-oxide.

$$C_2HCl_3 + 2O_2 \rightarrow HCl + Cl_2 + 2CO_2,$$

$$4HCl + O_2 \rightleftarrows 2Cl_2 + 2H_2O$$

The chlorine interacts with the rapidly moving deep lying impurities in the silicon, and removes them by conversion to their chlorides. This results in an improved lifetime in the silicon. Next, it is believed that chlorine is instrumental in the capture of the N_a^+ ions to form a neutral system. Thus, it effectively removes this high mobile charge species and so greatly improves the quality of the oxide and results in a reduction of the surface-state density at the $Si\text{-}SiO_2$ interface. It is also known to reduce oxidation enhanced diffusion and oxidation stacking fault generation.

3-4 Edge Effects in MINP Cells

MINP cells are very highly tuned to achieve high efficiency. Thus, any excess currents must be eliminated in order to meet the goal. Preparation of the edges of solar cells is a critical step. Initially, the cells were scribed with a diamond cutter and the edges dipped in acid to remove cutting damage. Currents were still too high with $J_{o\ell} \simeq 10^{-10} A/cm^2$. Later, a diamond saw was used to cleanly and precisely cut the cells and thus leave a high quality edge. This resulted in $J_{o\ell} \simeq 10^{-11}$ to 10^{-12} A/cm^2, at least an order of magnitude reduction in $J_{o\ell}$ to give improved V_{oc} and FF. Samples 765 and 769 of Table 5 have a high FF because of this new edge preparation technique.

More details concerning excess currents are given in Chapter 5.

3-5 Other Design Modifications and Discussion of the Most Efficient Cells

Table 5 contains data on textured cells represented by sample 770 which was typical of the others in that category. Texturing was accomplished by use of Solar Cell Etchant Type SCE-200 from Transene Co, into which a wafer was placed for 20-30 minutes at 80°C prior to ion implantation. Unfortunately, the back surface was also textured which we feel leads to a reduced fill factor and increased leakage currents. Texturing gave much better J_{sc} but lower V_{oc}, FF, and η. An increased effort in this area would certainly lead to an improved cell.

A minor effort was made to fabricate the MINP-P cell. This cell has 100-200 Å I-layer between grid lines and 20-25 Å I-layer under grid lines to reduce surface recombination. A pair of cells, 775 and 776, represent typical results from this study. The MINP-P cell did not offer an improvement. The A/R coating, grown before the thin I-layer, may lead to contamination of the surface prior to growth of the thin I-layer. Also, the photoresist process may have led to some contamination. Again, the non-optimum coating served to give reduced J_{sc} and η.

Data on the highest efficiency MINP and MNP-P cells are given in Tables 5 and 6. MINP cells were more efficient than MNP-P cells since the former had a more optimum A/R coating. Best efficiency values were 18.5% based on active area and 15.6% based on total area. Our best grid design had 6% shading. One of the best cells, #765, was implanted and annealed at Spire whereas the others were only implanted at Spire. This cell had extremely good values of J_{od}, $J_{o\ell}$, n_d and n_ℓ. The spectral response data for 3 of the best cells is given in Figure 10. Data are very consistent. Cell 765, implanted and annealed at Spire, was improved in the IR region meaning that the starting silicon wafer had a higher diffusion length or that the annealing process caused less degradation of the substrate. Finally, all cells were quite stable as shown in Table 6 for MINP, MNP-P-O, and MNP-P-T designs. MNP-P-T cells only degraded by 0.16% in V_{oc} and 1.37% in efficiency which shows an added benefit of Cl in the oxide. Also, MINP cells were stable when exposed to 100 mW/cm^2 UV for 16 days.

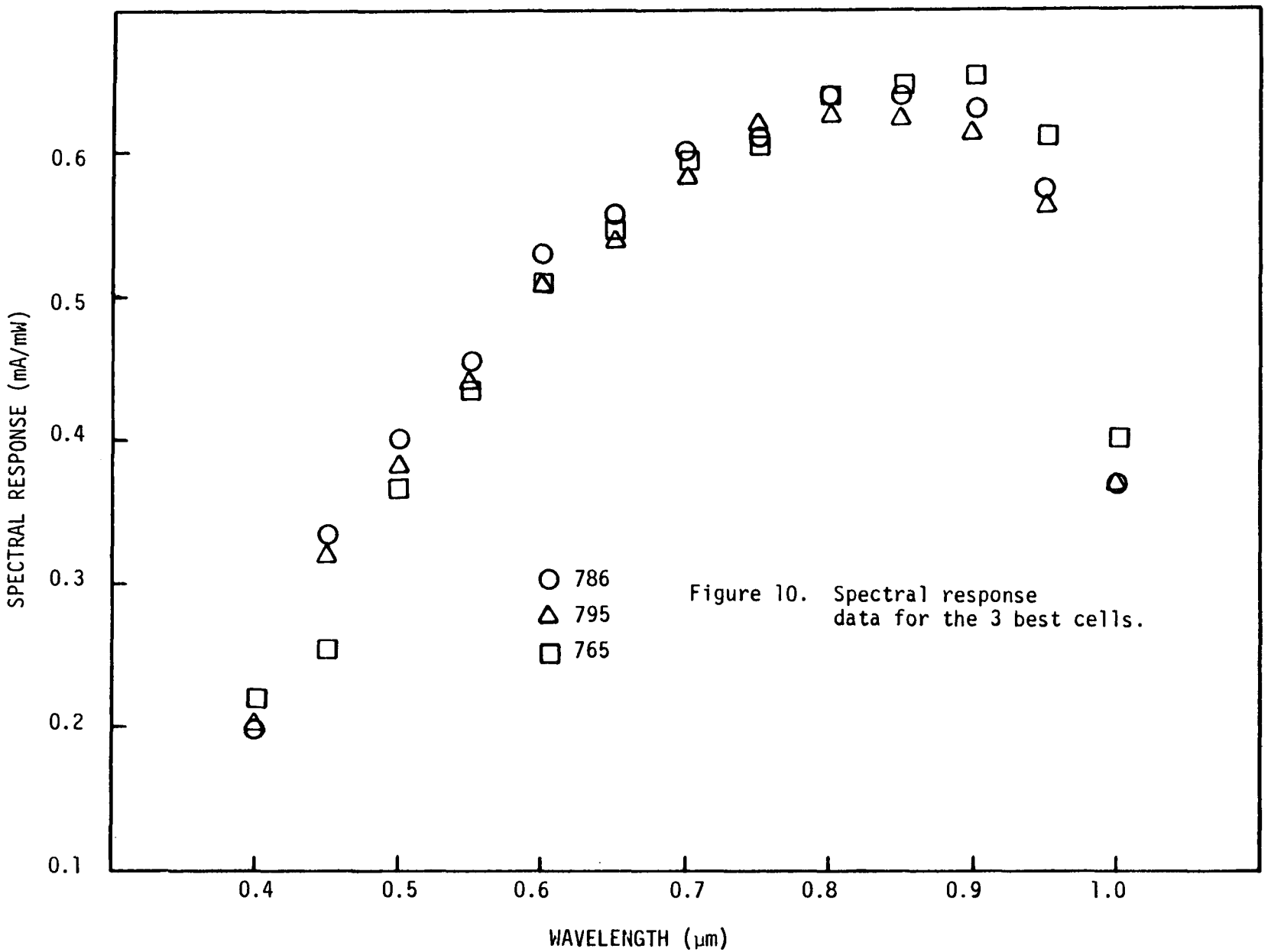

Figure 10. Spectral response data for the 3 best cells.

IV - DIFFUSED MINP CELLS

MINP solar cells with efficiency values between 16 - 18% have been reported where the n-layer was obtained by ion-implantation. This chapter reports on the fabrication of MINP solar cells with a low-cost diffusion technique using solid diffusion source transtar phosphorus PH-900 obtained from Carborundum. Efficiency values greater than 14% (total area) have been achieved.

After the preliminary cleaning of the wafers (1" x 1") they were etched in planar etch solution for approximately two minutes to reduce the thickness to $\sim$ 10 mils. To mask the back surface during diffusion, a 200 - 300 Å oxide layer was grown at $\sim$ 850 °C in dry oxygen. This was followed by a 700 Å thick silicon oxide layer deposited by thermal evaporation. Wafers were then vertically stacked with the solid source (without touching the surfaces), and subjected to diffusion at 800-950 °C for 5-20 minutes. The oxide from the back surface was finally stripped off prior to aluminum evaporation to make an ohmic contact. The aluminum layer was sintered at 580 °C while growing the top I-layer. A grid pattern was photolithographically defined and a sequence of metal layers consisting of Yb/Cr/Al thermally evaporated over the entire surface (including the unexposed photoresist). The metal pattern for the grid was finally obtained by a metal lift-off technique. A standard silicon oxide antireflection coating was deposited. The cells were finally finished by scribing and chemically etching the edges except for PDS-12 which was cut by diamond saw.

The photovoltaic parameters obtained on cells PDS-7, 9, and 12 are presented in Table 5. Figure 11 shows the spectral response of the cells reported herein. These cells show a better ultraviolet response than the standard P/N cell. However, the infra-red response is quite poor which can be attributed to the high temperature processes involved. This is further supported by the diffusion length measurements. We anticipate that the effect of oxidation is more severe; although the temperature during oxidation is lower than that for diffusion, the time involved in oxidation is longer than during diffusion. Furthermore, the diffusion parameters are not yet optimum which will make a difference in the cell performance. Studies underway in this direction include lower oxidation temperatures and optimization of diffusion parameters. Another possibility for reducing the damage during oxidation is to use low temperature oxidation (e.g., electrolytic oxide growth). These cells may have a considerably lower surface recombination velocity which can further improve the cell performance.

Benefits from the edge etching procedure are shown by the I-V data of Figure 12. It is clear that proper preparation of solar cell edges is essential to achieve high efficiency.

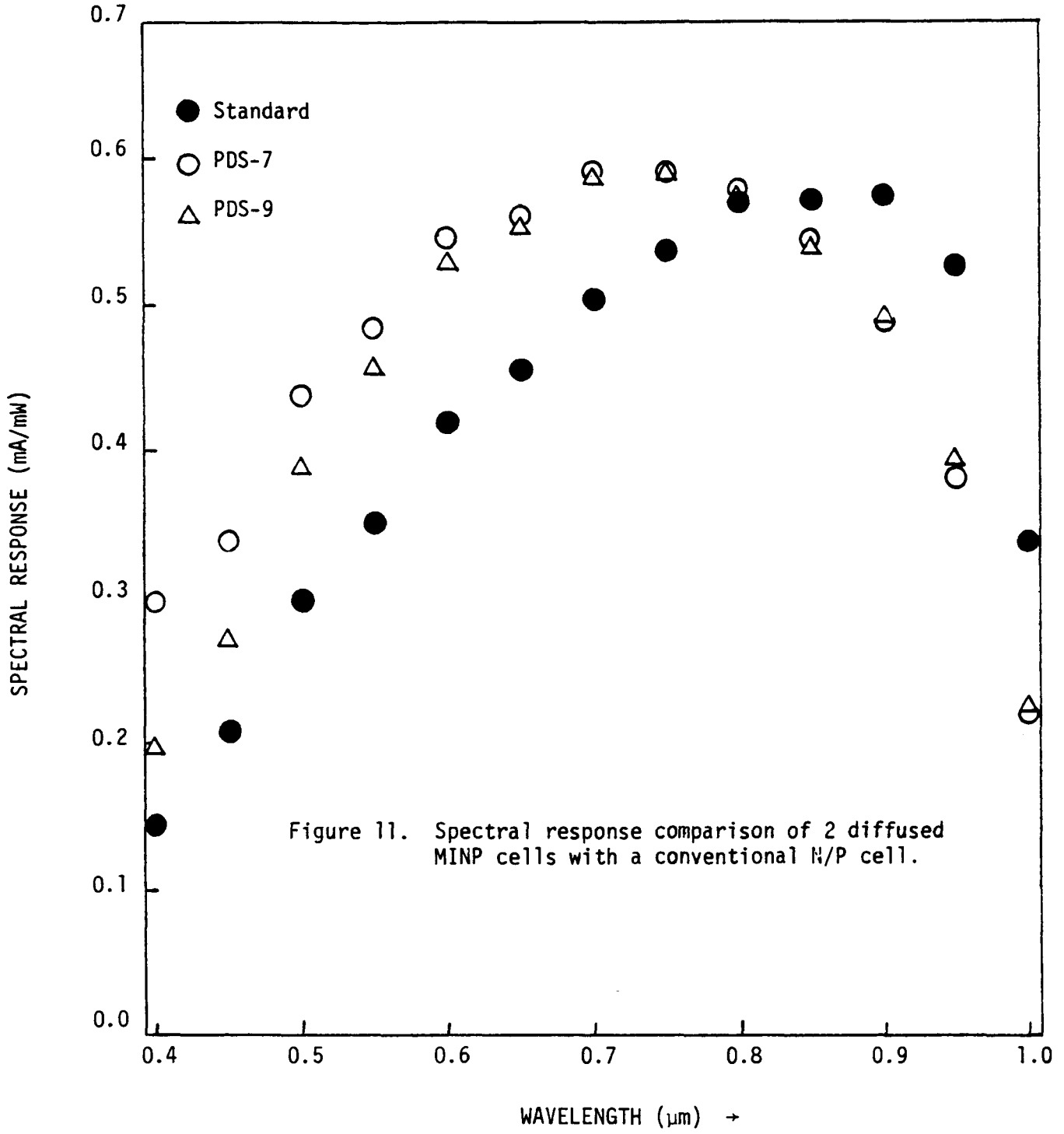

Figure 11. Spectral response comparison of 2 diffused MINP cells with a conventional N/P cell.

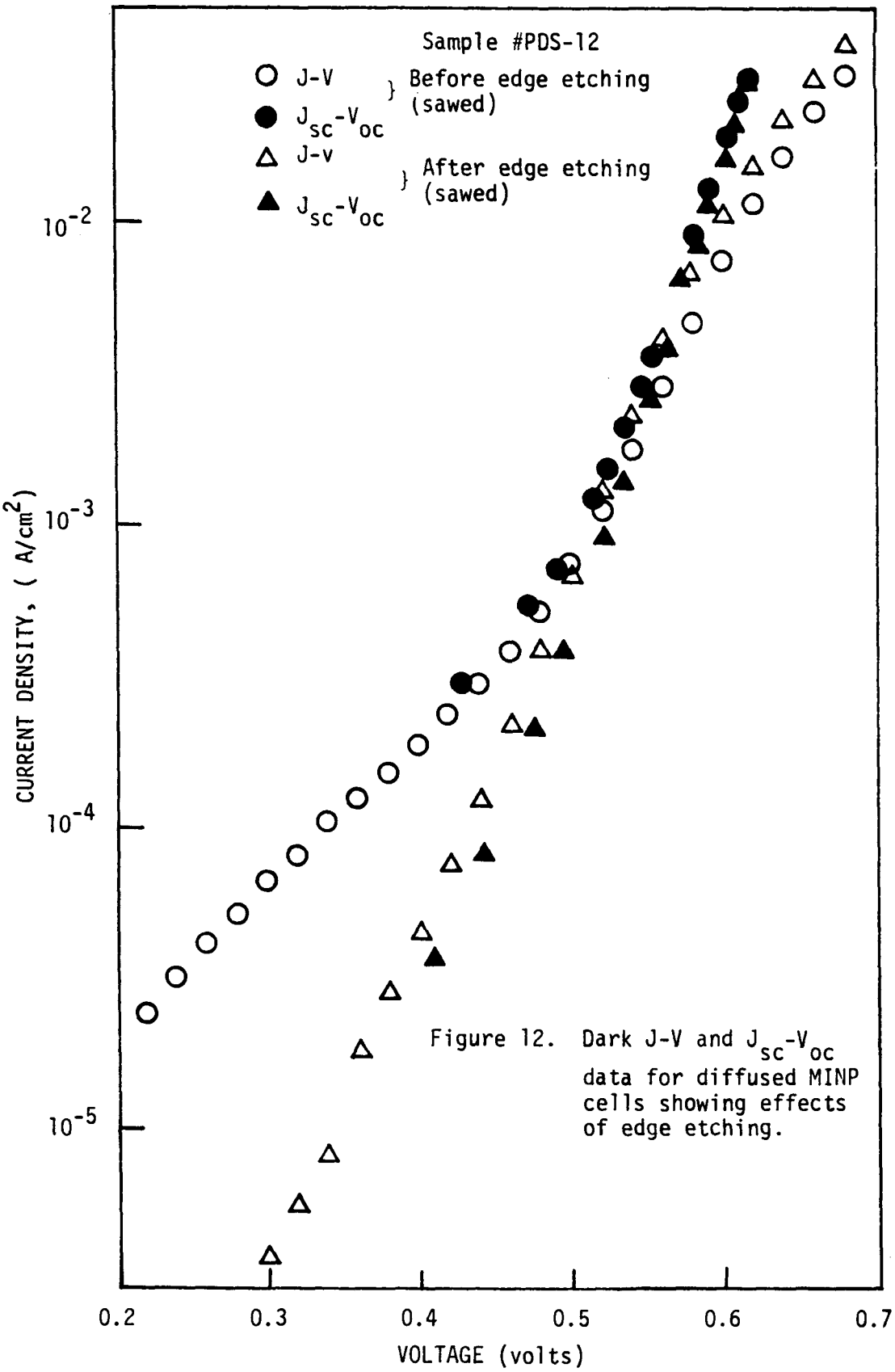

Figure 12. Dark J-V and J_{sc}-V_{oc} data for diffused MINP cells showing effects of edge etching.

V. EXCESS CURRENTS IN MINP-TYPE SOLAR CELLS

5-1 Experimental Data

I-V-T and I_{sc} - V_{oc} - T data were obtained for at least 2 samples of each of 4 kinds of cells shown in Table 7. Excellent reproducibility of data was obtained. The typical J-V-T and J_{sc} - V_{oc} - T curves are shown in Figures 13 and 14, respectively, for scribed plus etched MINP cells. All scribed plus etched cells gave much the same data. In fact, MNP, MINP, and MNP-P cells, whether diffused or implanted, gave much the same result and will not be emphasized here. Rather, the emphasis will be upon edge preparation techniques which control much of the excess currents in this study. These figures illustrate the nonlinear nature of dark characteristics whereas light characteristics are quite linear in the high voltage region, with an ideality factor close to 1.0 as predicted by and in support of simple diffusion theory. Dark J-V-T data contain the diffusion current component and excess currents such as those due to recombination. J_{sc} - V_{oc} - T data represent the diffusion component only since they are taken at high forward voltage and during illumination so that recombination centers are mostly filled. In Figure 14, the high voltage straight line portion may be extended downward to intersect the J_{sc} axis. This line now represents the diffusion component of current where the slope gives an ideality factor of about 1.0 and the J_{sc} axis intercept gives the diffusion component of reverse saturation current density, J_{od}. Each different temperature of Figure 14 results in a different J_{sc} - axis intercept and thus a new value of J_{od}. Each J_{od} value represents a key ingredient of the ideal diffusion equation

$$J_d = J_{od}[\exp(\frac{qV}{kT}) - 1] \qquad (11)$$

which is used in later calculations of the excess current equation.

TABLE 7

EXPERIMENTAL DATA FOR MINP-TYPE CELLS

Cell Number	Substrate Resistivity (Ω-cm)	V_{oc} (mV)	(a,c) J_{sc} (mA/cm^2)	Fill Factor	(a,c) AM1 Efficiency (%)	Activation Energy ϕ_1 (eV)	Activation Energy ϕ_2 (eV)	J_{oe} (A/cm^2)	(b) n_e (@ 295 °K)	dV_{oc}/dT (mV/°C)	(e) Type of Cell
729	0.3	613	30.5	0.73	13.6	0.43	0.89	3.4×10^{-6}	3.7	1.88	MNP (SC)
720	0.3	610	31.0	0.74	14.1	0.67	1.03	2×10^{-6}	3.3	2.0	MNP-P (SC)
730	0.3	624	32.0	0.73	14.4	0.48	0.94	8×10^{-6}	3.4	1.88	MINP (SC)
765 (e)	0.3	631	32.7	0.80	16.5	-	-	-	-	-	MINP (SA)
769	0.3	626	31.2	0.80	15.6	0.75	1.1	1.5×10^{-7}	2.6	-	MINP (SA)
11 A (SPIRE)	0.3	610	33.1 (d)	0.80	16.2 (d)	0.96	1.3	2×10^{-8}	2.3	-	N/P-P (SA)

a: Taken at 295 °K using an ELH lamp at 100 mW/cm^2.

b: n_e = ideality factor at 295 °K for the J_e current component

c: Based on a total area of 2.2 cm^2. Total area is 12% more than the active area.

d: Based on total area of 4.0 cm^2.

e: SC - scribed, SA - sawn.

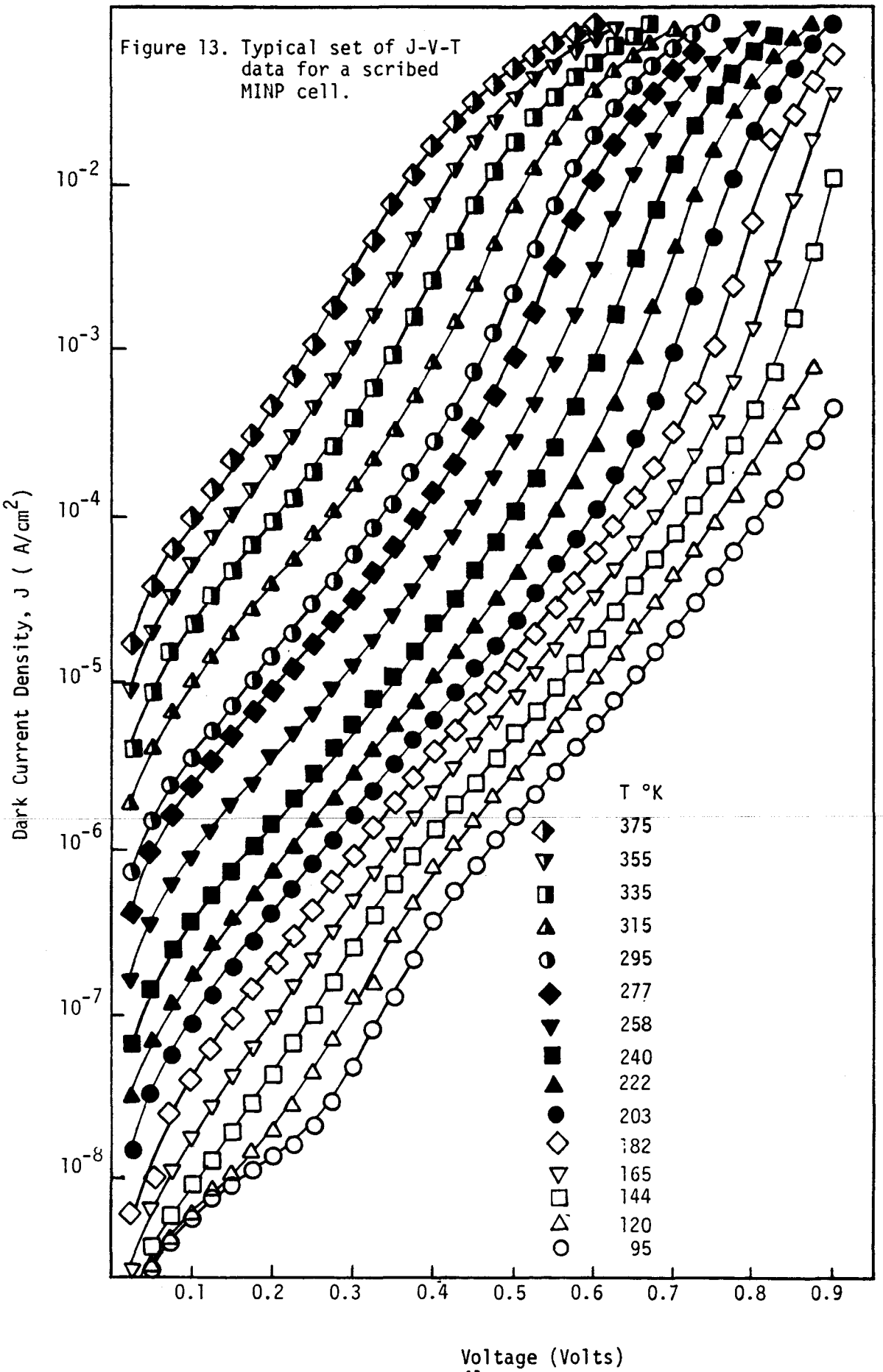

Figure 13. Typical set of J-V-T data for a scribed MINP cell.

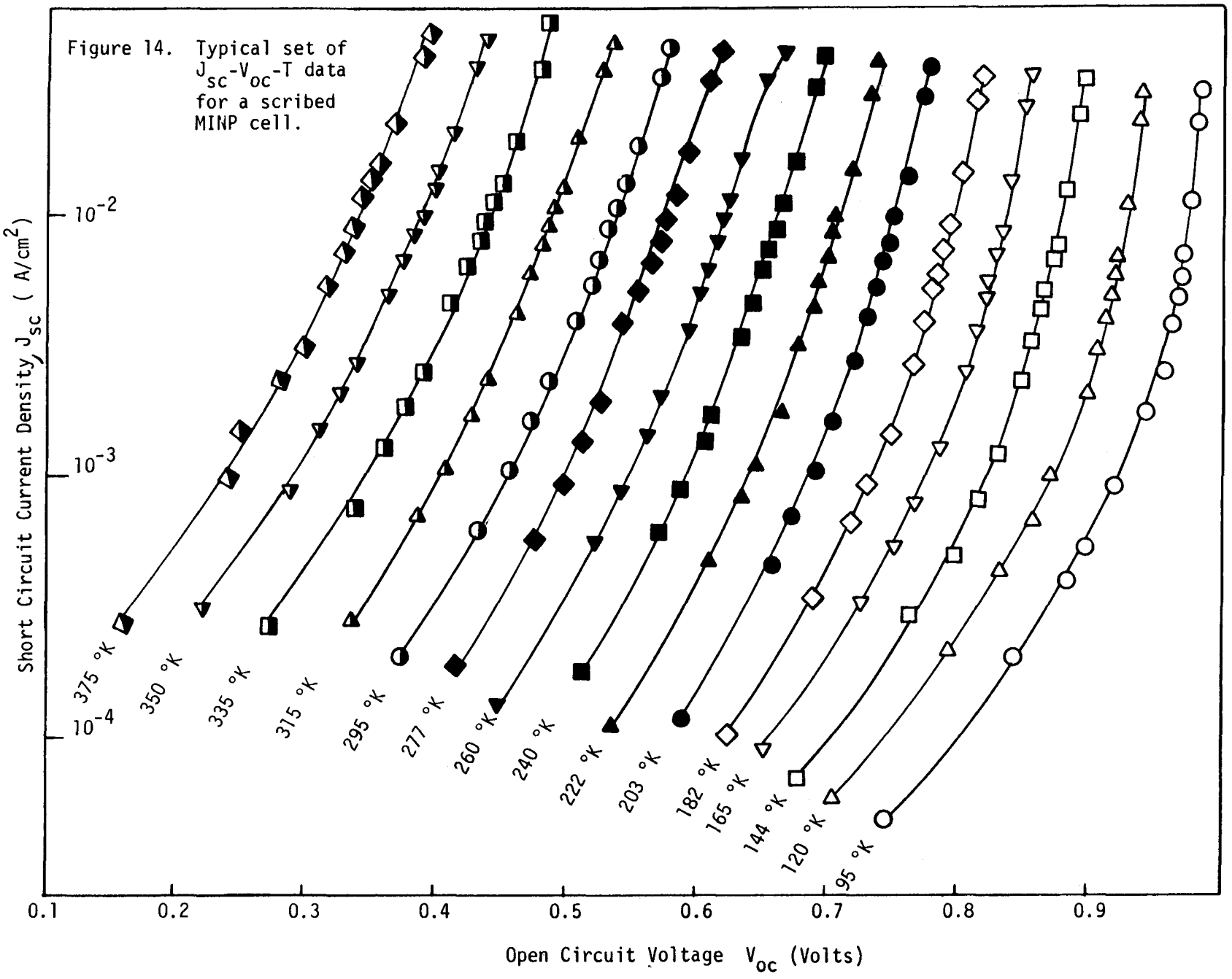

Figure 14. Typical set of J_{sc}-V_{oc}-T data for a scribed MINP cell.

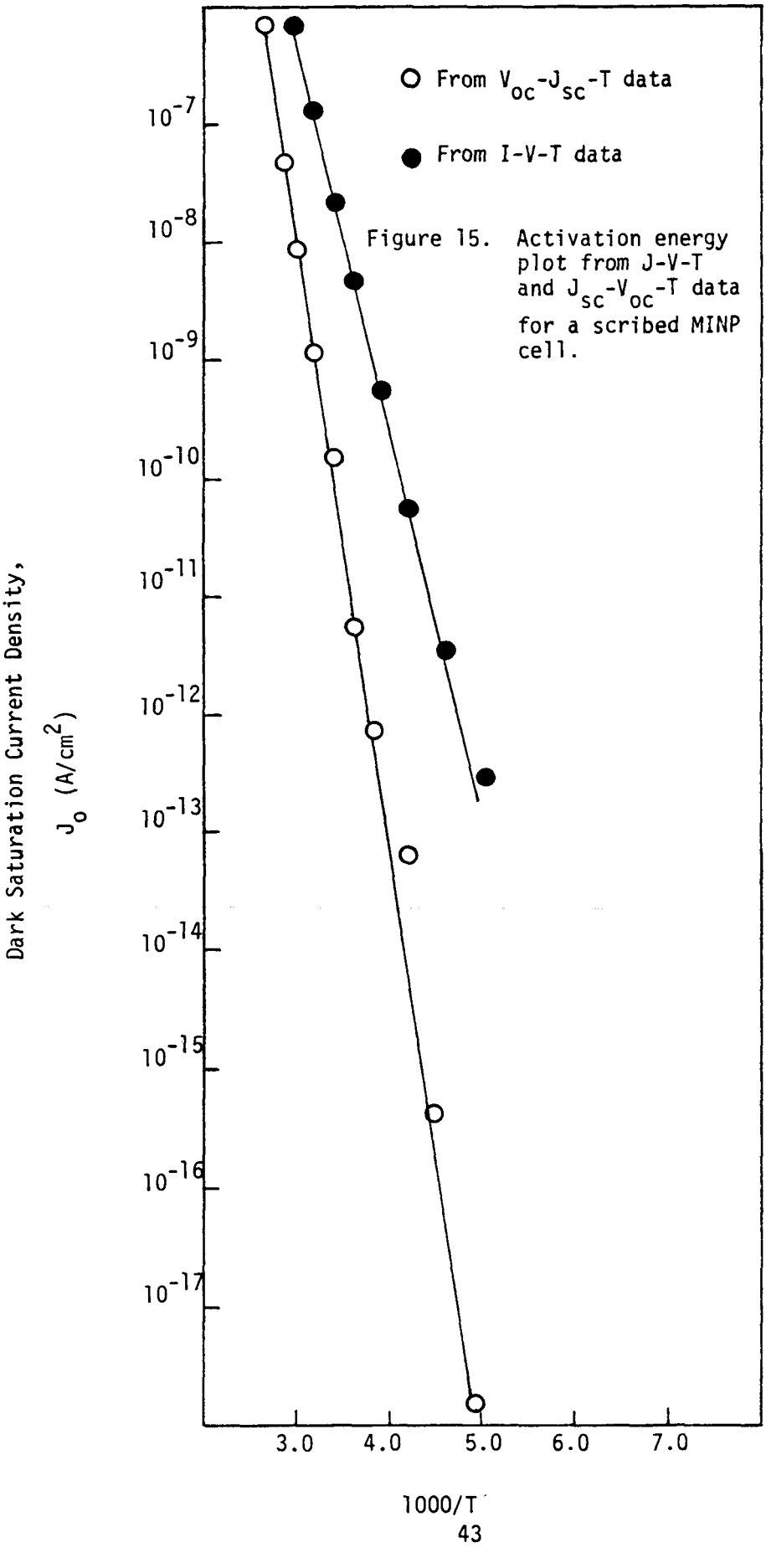

Figure 15. Activation energy plot from J-V-T and J_{sc}-V_{oc}-T data for a scribed MINP cell.

Activation energy, ϕ, may therefore be obtained from a plot of J_o vs. 1000/T as shown in Figure 15. The value of ϕ_2 (from J_{sc} - V_{oc} - T data) was obtained in each case by plotting J_{od} from J_{sc} - V_{oc} - T vs. 1000/T. The value of ϕ_1 was obtained from a similar analysis of the high voltage portion of curves in Figure 13. These results are also presented in Table 7 for the 4 cases.

In order to study the role of the excess current, the excess current density at the junction, J_e, was obtained using the equations

$$J = J_e + J_d = J_{oe}\left(e^{q(V-IR_s)/n_e kT} - 1\right) + J_{od}\left(e^{q(V-IR_s)/n_d kT} - 1\right) + \frac{V-IR_s}{R_{sh}} \cdot A \quad (12)$$

where J = total current density, J_e = excess current density, J_d = diffusion current density, J_{od} = reverse saturation value of diffusion current density, n_e = ideality factor for excess current, n_d = ideality factor for diffusion current, R_s = series resistance, and R_{sh} = shunt resistance. The equation including resistance effects may be solved for J_e

$$J_e = J - J_{od}\left[e^{q(V-IR_s)/n_d kT} - 1\right] + \frac{V-IR_s}{R_{sh}} \cdot A \quad (13)$$

J_{od} and n_d values were obtained from intercept and slope of J_{sc} - V_{oc} - T curves assuming the diffusion term to predominate at high voltage under illumination. In order to account for slight variations in R_s at different temperatures, R_s was obtained for each temperature and each cell using the technique described by M. Wolf.[20] R_{sh} for these cells was determined to be about 10^4 Ω using J_{sc} - V_{oc} data under very low illumination. Using $R_{sh} = 1 \times 10^4$ Ω and the aforementioned values of J_{od}, n_d, and R_s in equation 13, a family of J_e - V - T curves was generated as pictured in Figure 16 for sample 720. This family of curves was obtained by taking each

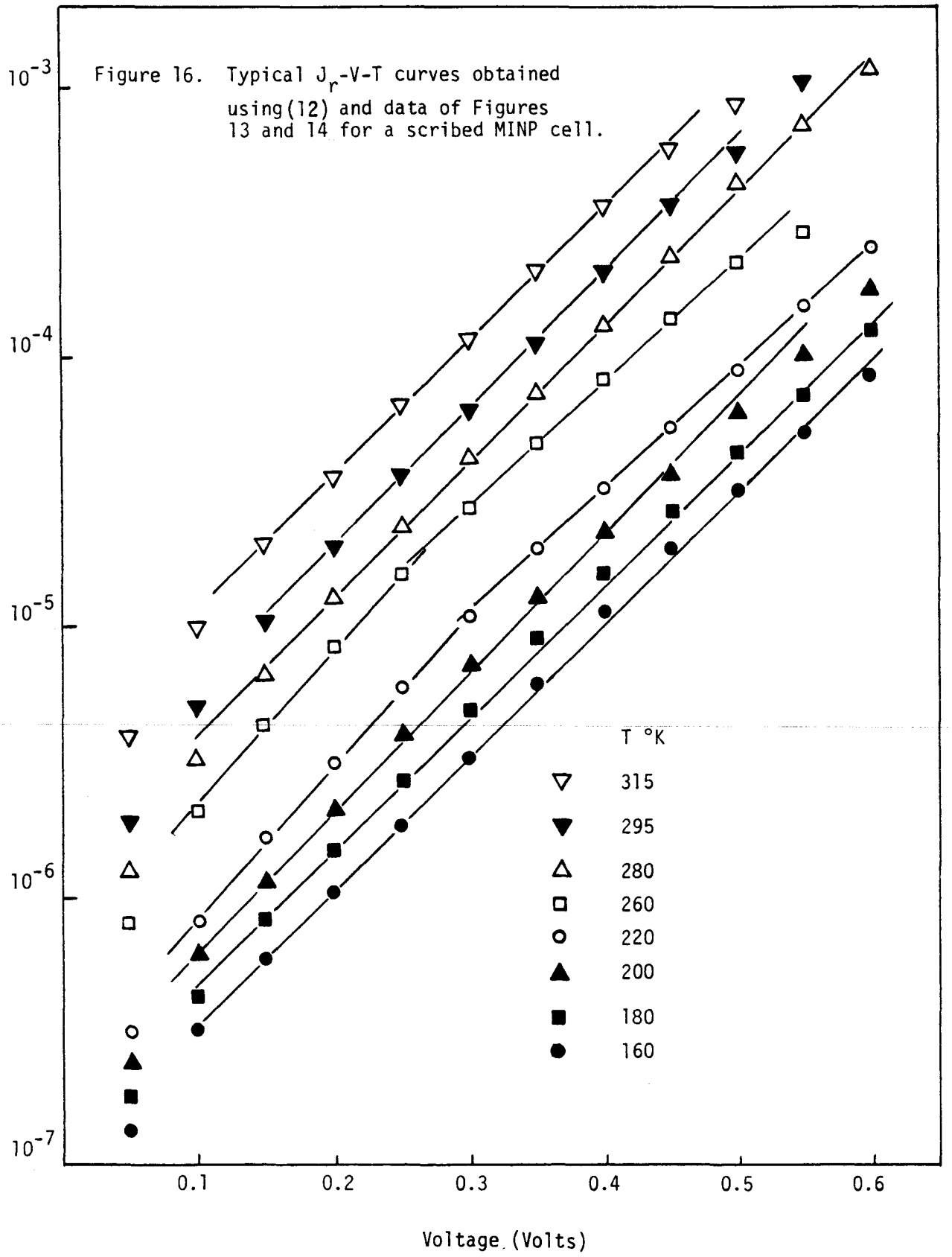

Figure 16. Typical J_r-V-T curves obtained using (12) and data of Figures 13 and 14 for a scribed MINP cell.

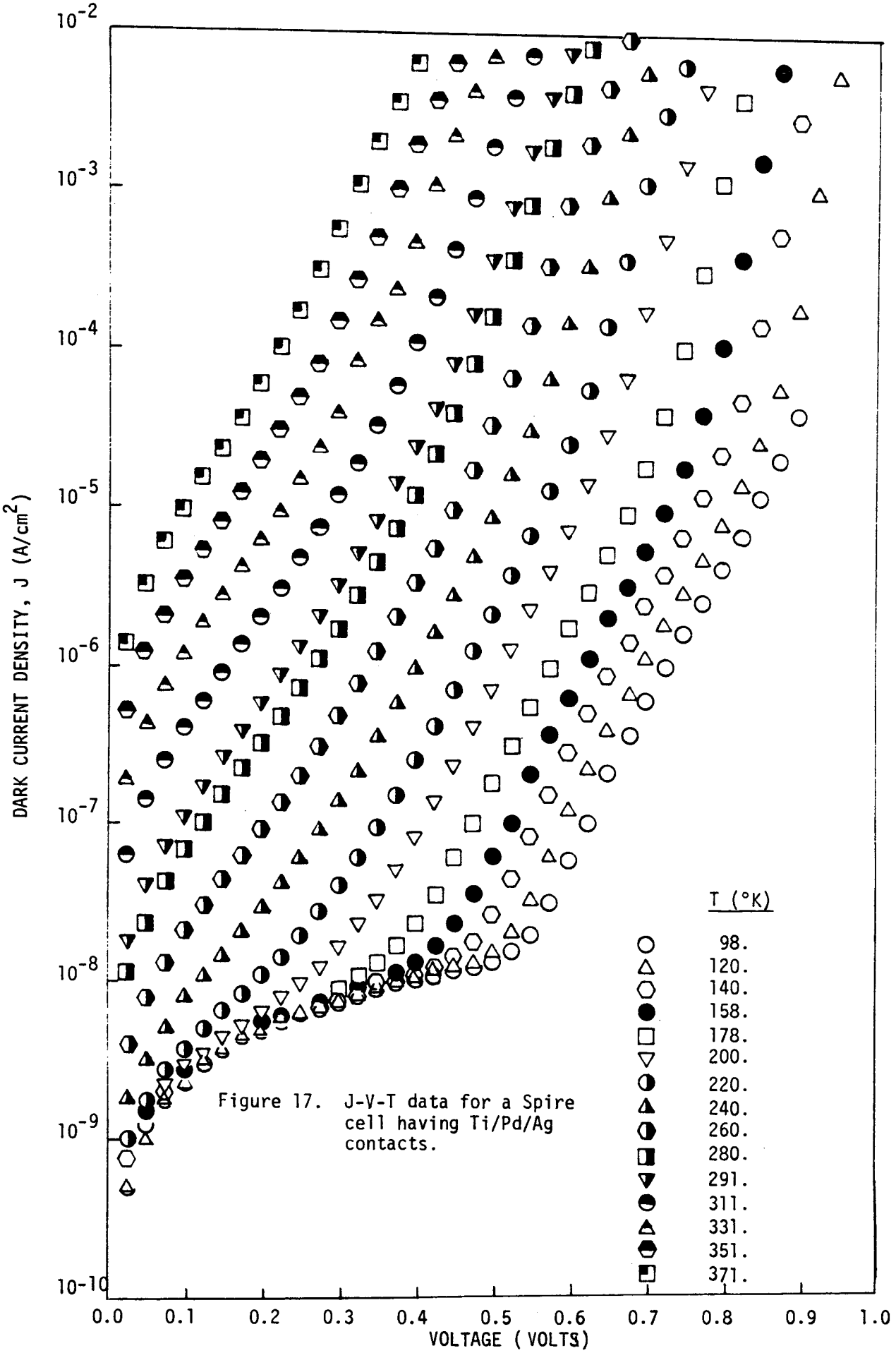

Figure 17. J-V-T data for a Spire cell having Ti/Pd/Ag contacts.

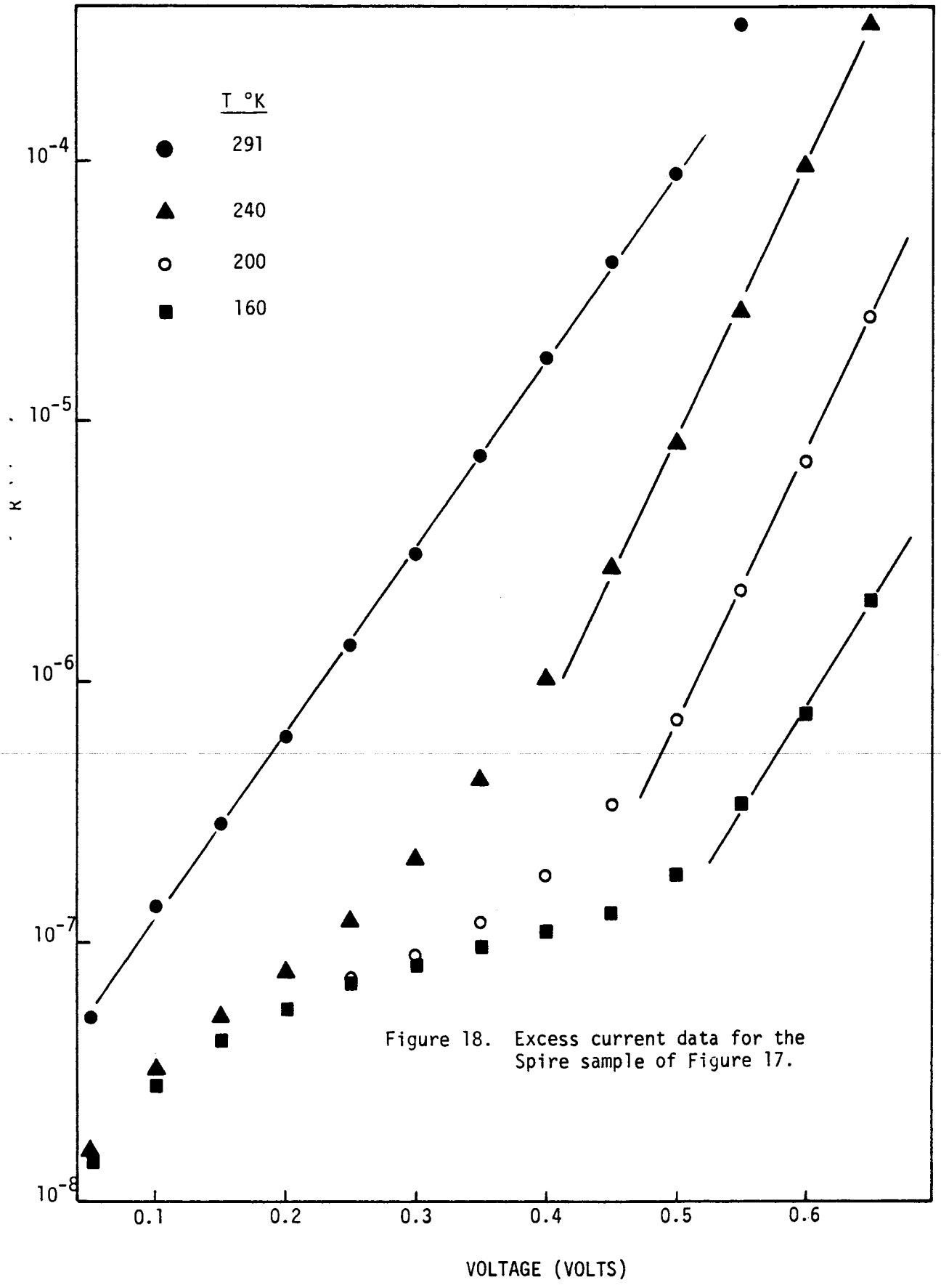

Figure 18. Excess current data for the Spire sample of Figure 17.

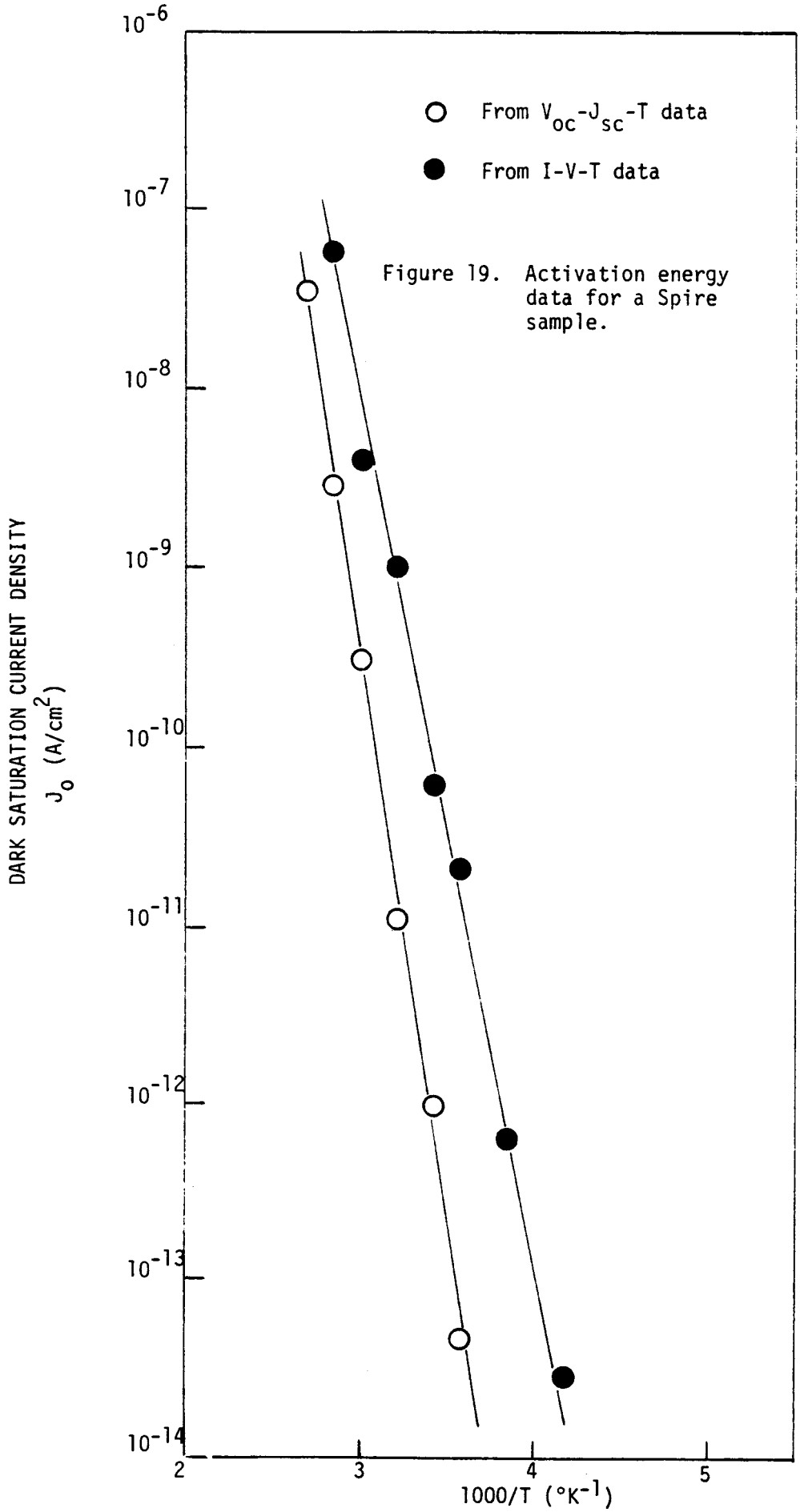

Figure 19. Activation energy data for a Spire sample.

J - V - T curve, as in Figure 13, and subtracting the diffusion term by computer at that temperature obtained from Figure 14 and represented by equation 11. The resulting excess current data of Figure 16 gave linear semilogarithmic behavior from which the J_e - axis intercept gave J_{oe} and the slope gave n_e. These values are also listed in Table 7. J_{oe} values in Table 7 were obtained for each case by extrapolating the linear region of the room temperature curves to the current axis using J_e-V-T data.

A similar set of data were taken for diamond sawn cells and Spire cells which gave significantly higher efficiency as listed in Table 7. J-V-T, J_e-V-T, and activation energy data for a typical Spire cell are shown, respectively, in Figures 17-19. Figure 17, compared to Figure 13, shows a much greater linear region and lower values of current at lower voltages. Figure 18, compared to Figure 16, shows a completely different temperature behavior and significantly lower current values. These differences are analyzed in the discussion.

5-2 Discussion

Four designs of high efficiency cells were evaluated for comparison of performance and evaluation of excess currents. Excess current data of Figure 16 resulted by subtracting the diffusion current component, calculated from J_{sc} - V_{oc} - T data of Figure 14, from the total current component, represented by J-V-T data of Figure 13. Excess current data of Figure 16 are described by J_{oe} $[\exp(qV/n_ekT) -1]$, over much of the voltage range, where straight line portions of the data are quite parallel. The parallel nature of this region requires n_eT = constant, or n_e = constant/T. If J_{oe} is due to recombination, then the theroetical expression for J_{oe} is given by[21]

$$J_{rt} = \frac{qn_i W(V)}{(\tau_{no}\tau_{po})^{1/2}} \left\{\frac{2\mathrm{Sinh}(qV/2kT)}{q(V_d-V)/kT}\right\} f(b) \qquad (14)$$

where W = depletion region width, f(b) = an integration factor,[21] and other terms have their usual meaning. The factor f(b) $\sim 10^{-2}$ for an asymmetrically doped n^+/p junction.

The ideality factor, n_e, should be about 2 and invarient with temperature for a recombination mechanism. Experimental values of J_{oe} are reported in Table 7 at T = 295°K. Here are listed values for scribed MINP cells of about 2-8 x 10^{-6} A/cm^2, for sawn MINP cells of 1.5 x 10^{-7} A/cm^2, and for Spire cells of 2 x 10^{-8} A/cm^2 compared to a theoretical calculation from equation 4 of 6 x 10^{-8} to 6 x 10^{-9} A/cm^2 using a range of typical values of the listed variables. The experimental values of J_{oe} for MINP cells are much too high to fit the recombination mechanism and n_e values are > 2. Data for Spire cells do much more closely agree with theoretical predictions indicating a recombination mechanism.

This behavior for MINP cells was reported by A. N. Saxena[22] in relation to MIS junctions. He defined a term

$$V_o = nkT/q \qquad (15)$$

in which V_o is independent of temperature for dominance of field emission. This fits the data of Figure 16 for a scribed MINP cell in which the slopes of the curves are essentially invariant with temperature. This theory also requires n_e to increase at decreased temperature and has been observed in highly doped metal/N-Si junctions where high field effects occur. This suggests J_e to be a field emission component rather than a recombination component for MINP cells. A combination of sawing and then etching is

required to reduce this component as shown in Table 7 for cell 769. The high efficiency Spire cells gave J_e values having a different temperature dependence and $n_e \simeq 2$ as shown in Figure 18. These data support a recombination current mechanism which is 100 times smaller than the field emission mechanism. These cells show near ideal behavior where the diffusion component is clearly dominant.

Table 7 contains data for several types of cells. The first three cells may be compared within the group since all were scribed. Oxide passivation for #720 and 730 gave highest efficiency. The efficiency of the MINP cell was highest of all due to the oxide under the grid as well as between grid lines. V_{oc} ranged from 610 - 624 mV for these cells. J_{oe} and n_e values were compared for all 3 cells indicating domination of edge effects even though efficiency was quite respectable. The second group of 3 cells were all of the sawn variety and thus gave higher fill factor and higher efficiency due to elimination of edge losses. J_{oe} and n_e values were much lowered compared to the first 3 cells indicating a small amount of recombination for the Spire cell and field emission for the MINP cell. Temperature variation of voltage for MINP cells was -1.88 mV/°K which is lower than the -2.3 mV/°K for typical N/P cells and in agreement with values reported by Green.[23] This increased stability in V_{oc} for MINP cells has also been observed while studying radiation effects in MINP cells and is presently being evaluated. Spectral response data indicates the superiority of MINP cells to the MNP-P variety since the I-layer also exists under the grid lines as well as between grid lines.

5-3 Conclusions

Diffusion current data were subtracted from total current to identify the excess current mechanisms in high efficiency passivated solar cells. This technique should also apply to other photo-sensitive devices. Scribed and etched MINP cells were limited in efficiency by a field emission mechanism evidenced by an ideality factor which increases at decreased temperature and a high value of saturation current. Sawn and etched MINP cells gave a reduced excess current which still fit field emission theory but gave high efficiency. Spire cells gave a recombination component of excess current as evidenced by a low value of J_{oe}, and an n_e value close to 2 which agree with theory. The low value of excess current in MINP and Spire cells gives an efficiency of 15.6 - 16.5% without multiple A/R, textured surface, or BSF. MINP cells are more efficient than MNP-P or N/P-P ones of a comparable structure since the I-layer also resides underneath the grid lines.

VI. RECOMMENDATIONS FOR FUTURE WORK

1. A further study of diffused MINP cells should be made using the solid source diffusant from Carborundum. This could be a low-cost, highly reproducible, low (850 °C) temperature process for solar cell fabrication.

2. More work is needed on true MINP cell design. Work of M. A. Green, Spire, and Westinghouse is on a passivated "violet" cell. Those cell designs do not evaluate different grid metals or the effect of an I-layer under the grid.

3. Different I-layers must be designed. It is quite likely that thermally grown SiO_2 is not the best. Further work on Cℓ-containing oxides should be a high priority.

4. Further work on low-temperature measurements will aid in identifying losses which limit efficiency.

5. The high efficiency design should be applied to lower-cost Si and poly-Si for an evaluation of required design changes. An I-V-T analysis should be applied to this study as well.

VII. REFERENCES

1. W. A. Anderson and A. E. Delahoy, "Schottky Barrier Diodes for Solar Energy Conversion," Proc. IEEE, 60, No. 11, 1457, November 1972.

2. W. A. Anderson, R. A. Milano, A. E. Delahoy and S. M. Vernon, "Recent Development in Schottky Barrier Solar Cells," J. Electrochem. Soc., 121, No. 8, 296C, August 1974.

3. S. M. Vernon and W. A. Anderson, "Temperature Effects in Schottky Barrier Silicon Solar Cells," Appl. Phys. Lett., 26, No. 12, 707, June 1975.

4. W. A. Anderson, A. E. Delahoy, and R. A. Milano, "Thin Metal Films as Applied to Schottky Solar Cells," Optical Studies, Appl. Optics, 15, No. 6, P. 1621, June 1976.

5. J. K. Kim, W. A. Anderson, and A. E. Delahoy, "Auger, Ellipsometry, and Environmental Studies of Thin Films Applied to Schottky (MIS) Solar Cells," Journal of Electronic Materials, Vol. 7, No. 3, pp. 403-413, May 1978.

6. S. K. Day, W. A. Anderson, A. E. Delahoy, and C. Cartier, "Spectral Response and Diffusion Length Studies of Amorphous, Polycrystalline, Ribbon, Epitaxial, and Single-Crystal Silicon MIS Solar Cells," Journal of Appl. Phys., Vol. 50, No. 6, pp. 4425-4430, June 1979.

7. W. A. Anderson, A. E. Delahoy, J. K. Kim, S. M. Hyland and S. K. Dey, "High Efficiency Cr-MIS Solar Cells on Single and Polycrystal Silicon," Applied Physics Letters, Vol. 33, No. 7, pp. 588-590, 1 October 1978.

8. K. Rajkanan, W. A. Anderson and G. Rajeswaran, "Loss Mechanism Analysis in Single and Poly-Si MIS Solar cells to produce a 13% Efficiency," Solar Cells, Vol. 3, pp. 17-25, 1981.

9. R. Ferraglio and W. A. Anderson, "Proton Radiation Effects on Cr-MIS Single Crystal Si Solar Cells," Appl. Phys. Lett., Vol. 35, pp. 18-20, 1 July 1979.

10. M. A. Green, A. W. Blakers, J. Shi, E. M. Keller, and S. R. Wenham, Appl. Phys. Lett., 44, 1163, 1984.

11. R. T. Young, G. A. Van der Leeden, R. L. Sanstrom, R. F. Wood, and R. D. Westbrook, "High Efficiency Si Solar Cells by Beam Processing," Appl. Phys. Lett., 43, pp. 666-668, 1983.

12. B. R. Appleton and G. K. Allen, Eds. "Laser and Electron Beam Interactions with Solids," North Holland, New York, 1982.

13. C. W. Shite and P. S. Percey, "Laser and Electron Beam Processing of Materials," Academic Press, 1980.

14. A. Gat, J. F. Gibbons, T. J. Magee, J. Peng, V. R. Deline, P. Williams and C. A. Evans, Jr., Appl. Phys. Lett., 32(5), 276, 1978.

15. A. Lietoila, J. F. Gibbons, T. J. Magee, J. Peng and J. D. Hong, Appl. Phys. Lett, 35(&), 532, 1979.

16. M. Y. Tsai, F. F. Morehead, J. E. E. Baglin and A. E. Michel, J. Appl. Phys., 51(6), 3230, 1980.

17. B. B. Rao, S. Banerjee, W. A. Anderson and M. K. Han, submitted to IEEE Trans. Elec. Dev.

18. M. B. Das, J. Stach, and R. E. Tressler, "Comparison Between HCl and TCE Grown Oxides on Silicon" J. Electrochem. Soc., 131, p. 389, Feb. 1984.

19. S. Solmi and P. Negrini, "Effect of Chlorine Implantation on Oxidation Enhanced Diffusion of Phosphorous in Silicon," Appl. Phys. Lett., 45, p. 157, 15 July 1984.

20. M. Wolf and H. Rauschenbach, "Series Resistance Effects on Solar Cell Measurements," Advanced Energy Conversion, April/June 1963.

21. A. L. Fahrenbruch and R. H. Buke, Fundamentals of Solar Cells, Academic Press, pp. 119-123, 1983.

22. A. N. Saxena, "Forward Current-Voltage Characteristics of Schottky Barriers on n-Type Silicon," Surface Science, 13, pp. 151-171, 1969.

23. M. A. Green, K. Emery and A. W. Blakers, "Silicon Solar Cells with Reduced Temperature Sensitivity," Electronics Letters, 18, pp. 97-98, 1982.

VIII. PUBLICATIONS

(1983 - 1984 ONLY)

8-1 Publications

1. G. Rajeswaran, V. J. Rao, M. A. Jackson, M. Thayer, W. A. Anderson and B. B. Rao, "A Stable Ytterbium - Insulator - Semiconductor Solar Cell Based on an Interface Degradation Model," IEEE Transactions on Electron Devices, 30, 12, p. 1840, December 1983.

2. M. Thayer, W. A. Anderson and B. B. Rao, "Reliability of MINP Compared to MIS, SIS and N/P Silicon Solar Cells Under 1.0 MeV Electron and Environmental Effects," IEEE Trans. on Elec. Dev., pp. 619-621, May 1984.

3. B. B. Rao, S. Banergee, W. A. Anderson, and M. K. Han, "Excess Currents in MINP-Type Solar Cells," submitted.

4. B. B. Rao, M. Jackson, and W. A. Anderson, "Improved Performance of Surface Passivated Devices by Cl-Containing Oxides," submitted.

8-2 Conference Presentations

1. B. B. Rao and W. A. Anderson, "Design Variables in MINP Solar Cells," Conference on Electron Device Activities in Western New York, Rochester, October 18, 1983.

2. *F. Y. T. Kai, M. A. Jackson, M. Thayer and W. A. Anderson, "Removing Grain Boundary Effects in Polycrystalline Silicon Using a Minority Carrier Mirror Concept," Material Research Society Annual Meeting, Boston, November 14-17, 1983.

3. W. A. Anderson, "Photovoltaics and Photoconductors," SUNY at Buffalo, High Technology Seminar Series, December 1983.

4. *B. B. Rao, S. Banerjee, W. A. Anderson and M. K. Han, "Excess Currents in High Efficiency Si Solar Cells," Proc. 17th IEEE Photovoltaics Specialists Conference, Orlando, May 1-4, 1984.

5. M. Thayer, S. Solaun, W. A. Anderson and B. B. Rao, "Radiation Effects in MINP and SIS solar Cells," Nuclear and Space Radiation Effects Conference, Colorado Springs, July 22-25, 1984.

*Proceedings Published

8-3 Dissertations & Thesis

1. F. Y. T. Kai, Grain Boundary Effects and Passivation Studies in Polycrystalline MIS Solar Cells, September 1983, Ph.D.
2. M. A. Jackson, Formation and Characterization of Electron Beam Deposited Silicon Films, September 1983, M.S.
3. S. A. Solaun, Radiation Effects on MINP Solar Cells, August 1984, M.S.
4. B. B. Rao, Processing Variable in Surface Passivated Silicon Solar Cells, in preparation.

IX. ACKNOWLEDGMENTS

Several people were quite helpful in the course of this work. Mark Spitzer of Spire Corp. shared in several technical discussions and provided silicon substrates. Wing Nip of Lumonics Corp. provided pulsed laser annealing services. H. S. Kwok of our department performed laser reflectance measurements. SIMS and Auger studies were conducted with the aid of Joe Gardella of our Chemistry Department, personnel of the NSF National Laboratory at Bozeman Montana, and John Dick of SERI. Solar cell photovoltaic measurements were performed at SERI and by Russell Hart at NASA Lewis Research Center. Charles Volk of Carborundum provided diffusion sources free of charge.

X. RESEARCH PARTICIPANTS

W. A. Anderson,	Principal Investigator
B. B. Rao,	Research Assistant (50% time)
S. Banerjee,	Research Assistant (50% time)
M. Jackson,	Research Assistant (10% time)
J. Bennett,	Clerical (5% time)